Reiter, K., Kukowski, N., Ratschbacher, L. (2011): The interaction of two indenters in analogue experiments and implications for curved fold-and-thrust belts. - Earth and Planetary Science Letters, 302, 1-2, 132-164

DOI: 10.1016/j.epsl.2010.12.002

Earth and Planetary Science Letters 302 (2011) 132-146

The interaction of two indenters in analogue experiments and implications for curved fold-and-thrust belts

Karsten Reiter[a,b,*], Nina Kukowski[b,1], Lothar Ratschbacher[a]

[a] TU Bergakademie Freiberg, Institute of Geology, Bernhard-v.-Cotta Str. 2, 09599 Freiberg, Germany
[b] GFZ German Research Centre for Geosciences, Telegrafenberg, 14473 Potsdam, Germany

ARTICLE INFO

Article history:
Received 9 May 2010
Received in revised form 15 November 2010
Accepted 1 December 2010
Available online 28 December 2010

Editor: Y. Ricard

Keywords:
4D analogue experiments
two indenter tectonics
particle image velocimetry
fold-and-thrust belts
Tajik basin
Pamir

ABSTRACT

Scaled analogue experiments are used to investigate the indentation of two basement blocks into a sedimentary basin and the formation of a fold-and-thrust belt. The experimental set-up has two adjacent indenters moving in parallel with a velocity difference. The slow indenter moves with a relative velocity ranging from 40 to 80% of that of the fast one.
In a first experimental series, quartz sand and low-friction glass beads represent the sediment stack and its basal detachment, respectively; silicone oil simulates a viscous detachment in the second series of experiments. The surface evolution and the spatio-temporal strain distribution are derived from particle image velocimetry (PIV). Together with the 3D finite structure derived by cutting the models at the end of each experiment, this allows the analysis of the structural evolution of the experimental wedges.
Thrusting wedge development depends crucially on the relative velocity: when the slow indenter moves with a velocity of more than 55% of the fast indenter, a single curved thrust wedge develops. The wedge becomes decoupled along strike-slip zone at large velocity differences, i.e. when the slow indenter moves slower than 55% of the faster indenter. Consequently the thrust front is strongly curved at high (55–60%) and smoothly curved at low velocity differences (70–80%); in all cases curvature increases during indentation. Along the most strongly curved portion of the thrust wedge, the transfer zone rises, particle rotation and material transport oblique to the indentation direction occur directed toward the front of the slow indenter. Thrusting cycles are timed by the fast indenter and influence thrusting in front of the slow indenter. Thrusts nucleate in front of the fast indenter wedge and propagate laterally to the slow indenter front. This implies distant effects of wedge growth active hundreds of kilometers along-strike of orogens.
Silicone oil as a detachment induces a low-angle wedge, which is less curved than in the glass beads experiments, and shows variable thrust vergence with fore- and back-thrusts. We compare our experimental results with the curved fold-and-thrust belts of the Tajik basin in front of the Hindu-Kush and Pamir indenters; our results are able to explain several first-order features.

1. Introduction

Foreland fold-and-thrust belts (FTBs) record pre- and syn-orogenic sedimentation and deformation between an orogenic core and its undeformed foreland. Many FTBs show foreland-directed deformation propagation, becoming younger with distance from the hinterland. The critical taper concept of *Dahlen et al.* (1984) and *Davis et al.* (1983) describes the mechanics of FTBs or accretionary wedges equivalent as to snow or sand wedges in front of an indenter. Accordingly, a wedge grows with a constant critical taper in a self-similar manner by accreting material via foreland-directed thrusting at its toe above a horizontal or inclined detachment according to the minimum work theory (*Masek and Duncan*, 1998). The material properties of the wedge and its detachment control wedge geometry. The latter might be modified by exogenic processes (sedimentation and erosion e.g. *Koons*, 1990; *Simpson*, 2010; *Storti and McClay*, 1995). A weak detachment with layers of evaporites or pore-fluid overpressure causes a thin-skinned FTB with a narrow taper, a dip angle of ≤1°, and inconsistent thrust vergence (e.g. *Davis and Engelder*, 1985).

Indentation tectonics illustrates the penetration of a rigid block into a weaker body and has been described at lithospheric scale for Anatolia (*Dewey et al.*, 1986) and Tibet (*Tapponnier et al.*, 1982), and at crustal scale for the Alps (*Ratschbacher et al.*, 1991a,b). Previous analogue experiments investigated the evolution of curved FTBs (*Calassou et al.*, 1993; *Cotton and Koyi*, 2000; *Keep*, 2000; *Lu and Malavieille*, 1994; *Macedo and Marshak*, 1999; *Marques and Cobbold*, 2002, 2006; *Marshak*, 2004; *Marshak and Wilkerson*, 1992; *Schreurs et al.*, 2001; *Zweigel*, 1998), focusing on indenter shape, thickness variations within the deforming layers, detachment rheology and lateral changes of detachment rheology and width of the layer stack (see also *Costa and Vendeville*, 2002; *Couzens-Schultz et al.*, 2003).

Inspired by ongoing studies of the Tajik basin (Fig. 1) of Tajikistan, Uzbekistan, and Afghanistan which showcases a curved FTB likely produced by one or more indenters, we investigate herein the evolution of curved FTB wedges that form in front of two parallel moving indenters advancing in the same direction (Fig. 2). In our experiments, the two indenters moved at different relative velocities and penetrated a layer stack of homogeneous sand above a detachment made of glass beads or silicone oil. We recorded the evolving model

* Corresponding author. GFZ German Research Centre for Geosciences, Telegrafenberg, 14473 Potsdam, Germany.
E-mail addresses: reiter@gfz-potsdam.de (K. Reiter), Nina.Kukowski@uni-jena.de (N. Kukowski), Lothar.Ratschbacher@geo.tu-freiberg.de (L. Ratschbacher).
[1] Present address: Friedrich Schiller University of Jena, Institute of Geosciences, Burgweg 11, 07749 Jena, Germany.

morphology via 3D particle image velocimetry (3D-PIV; e.g. *Adam et al.*, 2005; *Hampel et al.*, 2004) and calculated the displacement and rotation fields. As an application, we compare our modelling results with the first-order features of the Tajik-basin FTB, which is characterized by extreme width (≈ 300 km), strong curvature (90°) and development in front of two indenters, the Hindu Kush and the Pamir (Fig. 1C; *Bekker*, 1996; *Burtman and Molnar*, 1993; *Hamburger et al.*, 1992; *Keith et al.*, 1982; *Leith and Alvarez*, 1985). Furthermore, the adaptability of our experimental results to the structures of the Sulaiman Range is discussed.

2. Experimental set-up

2.1. Previous analogue indenter models of curved fold-and-thrust belts

During the last two decades, analogue experimental studies investigated the parameters potentially controlling the evolution of curved FTBs, for overview see *Marshak* (2004). Indenters (push experiments) with a step in their leading edge or with an angular shape create curved thrust wedges with thrust fronts, curving convexly and/or concavely toward the foreland mimicking the indenter shape (Fig. 3A–C; *Calassou et al.*, 1993; *Keep*, 2000; *Lickorish et al.*, 2002; *Macedo and Marshak*, 1999; *Marques and Cobbold*, 2002, 2006; *Marshak*, 2004). In these experiments, the wedges become progressively less curved during indentation in the transfer zone. An oblique indenter front (versus the motion) generates oblique fore-thrusts with a concavely or convexly curved wedge shape (Fig. 3B and C; *Calassou et al.*, 1993; *Lu and Malavieille*, 1994; *Zweigel*, 1998). This wedge tears with increasing convergence, localizing deformation in front of the leading corner (Fig. 3F; *Zweigel*, 1998). The rotation (or displacement gradient) of the indenter front (Fig. 3D; *Ghiglione and Cristallini*, 2007; *Lickorish et al.*, 2002; *Wilkerson et al.*, 2002) as well as a rigid obstacle within the basin (Fig. 3E; *Keep*, 2000; *Lickorish et al.*, 2002) are possible reasons for non-linear deformation within a FTB. Similar deformation pattern to obstacles is figured out in models, researching subduction of sea mount chains in accretionary prisms (*Dominguez et al.*, 1998, 2000; *Hsui and Youngquist*, 1985; *Lallemand et al.*, 1992). Lateral variations of

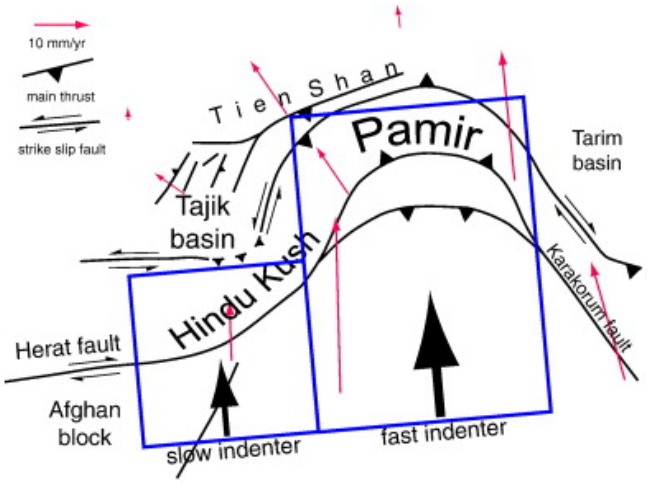

Figure 2. Hypothesis of two indenters: The Pamir is represented by a fast indenter and the Hindu Kush by a slow one, both could have generated the curved fold-and-thrust belt within the Tajik basin. Red arrows depict GPS-velocity vectors with respect to Eurasia (from *Mohadjer et al.*, 2010).

layer thickness or a lateral/oblique ramp (Fig. 3G; *Calassou et al.*, 1993; *Macedo and Marshak*, 1999; *Marques and Cobbold*, 2002, 2006; *Marshak and Wilkerson*, 1992; *Wilkerson et al.*, 2002) affect wedge growth and may also result in a bended wedge front with increasing curvature during convergence or wedge separation. A similar behaviour was observed in experiments with lateral changes in detachment rheology (Fig. 3H; *Calassou et al.*, 1993; *Cotton and Koyi*, 2000; *Keep*, 2000; *Macedo and Marshak*, 1999; *Schreurs et al.*, 2001).

Macedo and Marshak (1999) classify parameter controlling the generation of curved FTBs, where basin controlled salients have an increasing curvature during indentation. In contrast indenter controlled salients exhibit decreasing curvature while indentation. This could be indicated by convergent trend lines at the apex (smallest radius of curvature) of the salients (indenter controlled) or divergent trend lines at the apex (basin controlled). However, the generation of a curved wedge with increasing curvature is impossible with previous set-ups by in-

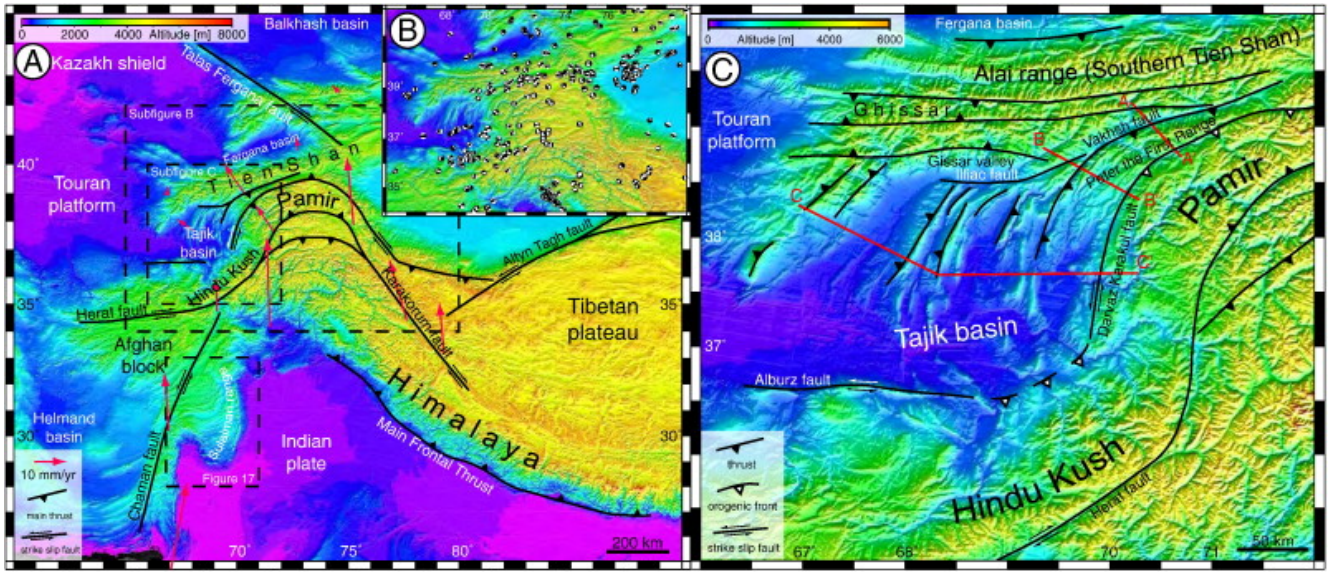

Figure 1. Morphotectonic map of Central Asia with first-order faults. Red arrows indicate GPS-velocity vectors with respect to Eurasia (from *Mohadjer et al.*, 2010), dashed lines locate areas shown in more detail in B and C. Structures compiled from *Koulakov and Sobolev* (2006) and *Robinson et al.* (2004). B) Map of seismicity in the vicinity of the Tajik basin showing seismic activity north of the Pamir and the Hindu–Kush. Focal mechanisms from Harvard catalogue. C) Topographic map of the Tajik basin with main faults. The red lines indicate the location of the cross-sections, represented in Fig. 16. Structures compiled from *Coutand et al.* (2002) and *Thomas et al.* (1994a), topography for all maps from GINA (*Linquist et al.*, 2004).

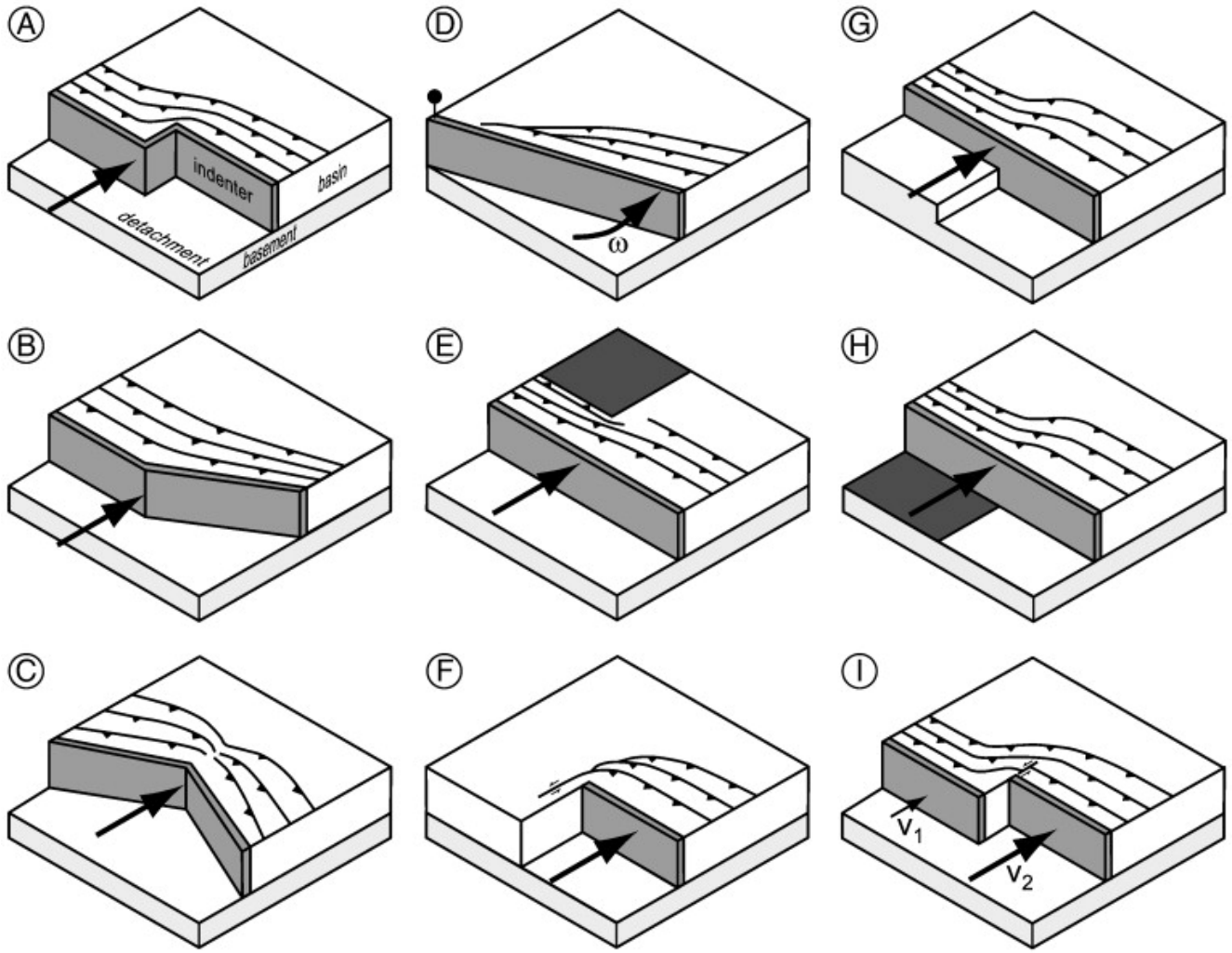

Figure 3. Illustration of possible parameters providing the generation of curved fold-and-thrust belts; indenter experiments are mostly a combination of more than one parameter. A–C) indenter shape: A) horizontal offset of the indenter (*Calassou et al.*, 1993; *Macedo and Marshak*, 1999), B) oblique indenter (*Calassou et al.*, 1993; *Lu and Malavieille*, 1994; *Macedo and Marshak*, 1999; *Zweigel*, 1998), C) convex indenter (*Lickorish et al.*, 2002; *Macedo and Marshak*, 1999; *Zweigel*, 1998) D) rotating indenter (e.g. *Ghiglione and Cristallini*, 2007; *Lickorish et al.*, 2002; *Wilkerson et al.*, 2002), E) obstacle within the basin (black region is more rigid then the basin - e.g. *Keep*, 2000; *Lickorish et al.*, 2002), F) leading edge of the indenter (*Zweigel*, 1998), G) lateral variation of basin thickness down to the detachment (*Calassou et al.*, 1993; *Macedo and Marshak*, 1999; *Marques and Cobbold*, 2002, 2006; *Marshak and Wilkerson*, 1992; *Wilkerson et al.*, 2002), H) lateral variation of detachment rheology (weaker detachment to the right - e.g. *Calassou et al.*, 1993; *Cotton and Koyi*, 2000; *Macedo and Marshak*, 1999; *Schreurs et al.*, 2001), I) two indenters with different velocities $\boldsymbol{v_1}$ and $\boldsymbol{v_2}$ (this study).

dentation in a homogeneous layer cake (indenter controlled).

Here we use so called flat indenters/backstops that have the same height or are lower than the deforming layer and become partly covered by the deforming material during the model run (Fig. 4A; *Bonini et al.*, 1999; *Byrne et al.*, 1988; *Koons*, 1990; *Lu and Malavieille*, 1994; *Persson and Sokoutis*, 2002; and *Persson et al.*, 2004). The latter set-up also permits the development of bivergent orogenic wedges. A deformable "effective indenter" develops at the indenter front (*Bonini et al.*, 1999; *Persson and Sokoutis*, 2002) with a single back thrust that enables material to flow onto the indenter.

2.2. Set-up of the sandbox experiments

Our set up used two adjacent rigid plates, moving in parallel, displaced with variable velocities that indent into a deformable horizontal layer cake made of granular material (Fig. 3I). We used wooden plates with a length of 35 cm and the same initial thickness as the sand and décollement pile (18 or 20 mm); the fast indenter had a width of 40 cm, the slow is 60 cm wide (Fig. 4B). Both indenters were pushed forward by thread rods driven by electrical motors. We simplified the stratigraphy of a sedimentary basin with a basal detachment to a homogeneous, deformable layer above a weaker horizon (Fig. 4A). We performed two experimental series: in the first we used a granular material at the base and tested the influence of velocity contrasts between the indenters on the structural evolution of the salient. A second series of experiments used a constant velocity contrast and tested the influence of a viscous detachment; this set-up resulted in a structure most similar to our case study area (Tajik basin). All models were built atop a rigid horizontal plate, which represents the autochthonous basement of the basin.

2.3. Material properties and scaling

We modelled the sediments on top of the basal detachment by 15 mm thick dry quartz sand, a Mohr–Coulomb material with negligible cohesion and a linear stress–strain relationship up to failure (Table 1; *Byerlee*, 1978; *Schellart*, 2000). Strain hardening occurs prior to failure (peak strength) with subsequent strain softening until steady-state shear strength (dynamic friction) (*Chu*, 1995; *Lohrmann et al.*, 2003; *Schanz and Vermeer*, 1996). The strength up to failure is controlled by cohesion and peak friction (μ_{peak}); static-stable friction (μ_{stat}) provides the strength of previously deformed material (reac-

tivated static friction), and dynamic friction (μ_{dyn}) is the strength of an active shear zone.

FTBs in nature, like the Cordilleran FTB, Sulaiman Range, Tajik basin, Jura Mountains, or Appalachian Plateau have a length of 200 to 800 km and a width of 100 to 500 km. Given the 100 × 100 cm model size (Fig. 4B) and the width of our indenters versus a natural analogue, we used a geometric scaling factor of 5×10^5 (i.e. 1 cm correspond to 5 km). Parameters of an assumed natural prototype (N), the analogue model (M), and the resulting scaling ratios (N/M) are listed in Table 2. To improve visualization, the sand is interlayered with a red sand marker horizon (Fig. 4A), which does not modify the bulk material properties significantly. For the first experimental series, a 3 mm thick layer of glass beads, a Mohr–Coulomb material with an ≈20% lower friction than sand (Table 1), was used to represent the detachment. The layer thickness of the glass beads is badly scaled (Table 2), because using glass beads requires a minimum layer thickness in order to localize shear. Both sand and glass beads were sieved onto the modelling table.

Several FTBs were formed by thin-skinned deformation atop a weak detachment (evaporites or layers with pore-fluid overpressure - e.g. *Davis and Engelder*, 1985; *Macedo and Marshak*, 1999). Rock salt has strain-rate dependent deformation behaviour with brittle failure occurring at high and viscous flow at low strain rates. We used silicone oil to model a viscous weak layer in the second series of experiments. The effective viscosity of the quasi-Newtonian-viscous silicone oil is $2.6 \pm 0.1 \times 10^4$ Pa s at the strain rates occurring in our experiments. The viscous behaviour requires proper scaling for velocity (v) (*Hubbert*, 1937; *Weijermars and Schmeling*, 1986): Viscosities of evaporitic rocks are in a range of 10^{17} to 10^{19} Pa s (*Clark*, 1966 cited in *Cotton and Koyi*, 2000; *Couzens-Schultz et al.*, 2003;). The appropriate convergence rate v_N is then calculated after *Weijermars and Schmeling* (1986) with gravity (g), thickness (l), density (ρ_d), and viscosity (η) of the detachment horizon:

$$v_N = \frac{\eta_M \times \rho_{dN} \times g_N \times l_N^2 \times v_M}{\eta_N \times \rho_{dM} \times g_M \times l_M^2} \quad (1)$$

The convergence rate of the fast indenter used in the experiments was 2 cm/h and is therefore scaled to nature to be between 1490 mm/yr ($\eta = 1 \times 10^{17}$ Pa s) and 8.4 mm/yr ($\eta = 1.7 \times 10^{19}$ Pa s); the latter is on the order of typical convergence rates in nature. We used a velocity (v_N) of 15 mm/yr for calculation.

Table 1
Physical properties of granular analogue materials used in experiments at the German Research Centre for Geosciences (GFZ); after *Hoth et al.* (2006).

Properties	Sand	Glass beads
Grain size (μm)	≤630	300–400
Peak friction μ_{peak} (strength of the undeformed material up to failure)	0.71 ± 0.01	0.56 ± 0.01
Static-stable friction μ_{stat} (strength of previously deformed material)	0.57 ± 0.01	0.47 ± 0.01
Dynamic-stable friction μ_{dyn} (strength in an active shear zone)	0.54 ± 0.01	0.41 ± 0.01
Cohesion C (Pa)	< 180	< 80
Strain softening (%)	20	13

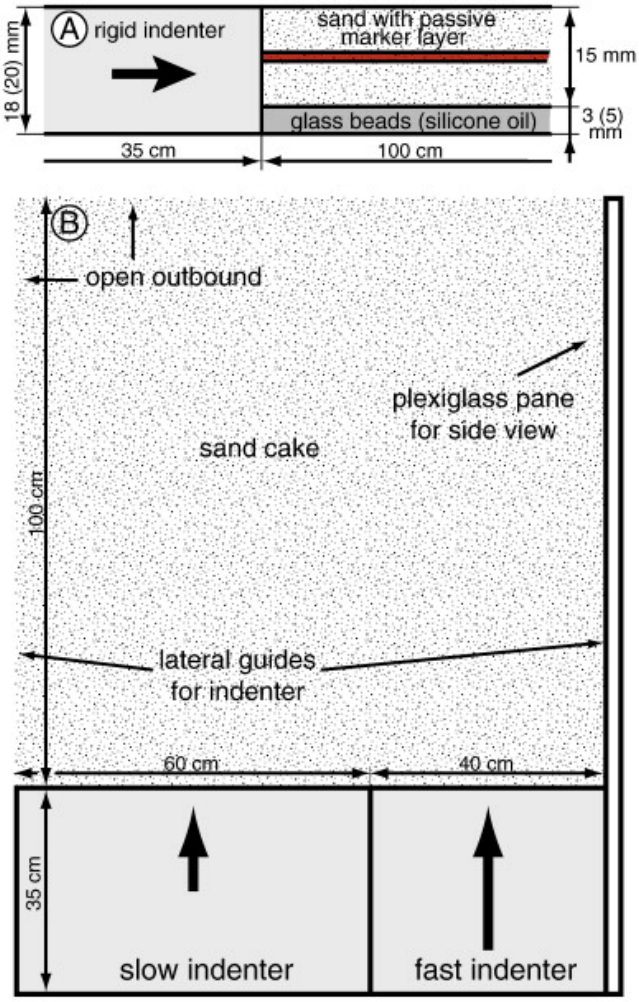

Figure 4. A) Mechanical stratigraphy, consisting of glass beads for the detachment in the first series (or silicone oil in the second series, dimensions in brackets) and a sand layer with a passive marker horizon in front of the flat indenter. B) Experimental set-up in map view.

2.4. 3D-particle image velocimetry (3D-PIV) and strain analysis

In the absence of surface mass wasting, deformation of an analogue model is reflected directly at the surface. Therefore, the evolution of the latter was our primary focus. To achieve this, we used 3D particle image velocimetry (3D-PIV; *Adam et al.*, 2005; *Arroyo and Greated*, 1991; *Hampel et al.*, 2004; *Prasad*, 2000), employing a stereoscopic camera set-up. We recorded all experiments with two 14 bit monochromatic Charge Coupled Device (CCD) cameras with a resolution of 11 million pixels at a frequency of 1 Hz. To optimize optical correlation, we mixed the sand with 8% of black sand. After each experimental run, the model was covered with black sand in order to stabilize structures and drizzled with ≈4.5 l water to reach saturation at a moisture of ≈25 vol.% (pore space filled). Then, we cut vertical sections through the deformed layer cake to observe the internal structure.

3. Results

3.1. Relative velocity experiments with glass beads décollement

In the first experimental series that consists of seven runs and in which six different velocity ratios between the two indenters were tested, we used glass beads for the décollement. One velocity-ratio experiment was run twice to confirm reproducibility; we did not observe significant differences. The fast indenter (FI) moved with a velocity of 2 cm/min (120 cm/h), the slow one (SI) with a velocity between 40 and 80% of that of the FI (Table 3). All experiments were stopped after a FI convergence of 60 cm.

Table 2
Scaling of analogue models for the first experimental series with the glass beads detachment and the second series with silicone oil detachment.

	Properties	Nature (N)	Model (M)	Scaling factor
Sediment succession modelled by quartz sand	Width of fast indenter (m)	2×10^5	0.4	5×10^5
	Width of the basin (m)	3×10^5	0.6	5×10^5
	Indentation into basin (m)	3×10^5	0.6	5×10^5
	Thickness of basin l (m)	7.5×10^3	1.5×10^{-2}	5×10^5
	Density ρ (kg m^{-3})	2.4–2.7[a]	1.74±0.01[b]	1.4
Evaporites modelled by glass beads	Thickness l (m)	600	3×10^{-3}	2×10^5
	Density ρ (kg m^{-3})	2.2[c,d]	1.59±0.01[b]	1.4
Evaporites modelled by silicone oil	Thickness l (m)	600	5×10^{-3}	1.2×10^5
	Density ρ (kg m^{-3})	2.2[c,d]	1	2.2
	Viscosity η (Pa s)	1.7×10^{19}[d]	$2.6\pm0.1 \times 10^4$	6.5×10^{14}
	Gravity g (m s^{-2})	9.81	9.81	1
	Velocity v (m s^{-1})	4.76×10^{-10} (1.5 cm yr^{-1})	5.56×10^{-6} (2 cm h^{-1})	8.6×10^{-5}
	Strain rate ε (s^{-1})	7.93×10^{-13}	1.11×10^{-3}	7.1×10^{-10}
	Stress σ (Pa)	1.35×10^7	2.89×10^1	4.7×10^5

[a] Estimated.
[b] *Hoth et al.* (2006).
[c] *Weijermars et al.* (1993).
[d] *Cotton and Koyi* (2000).

3.1.1. Evolution of the wedge(s) in front of the indenters

Following initial compaction of the granular material, fore- and back-thrusting allowed a pop-up structure to develop. In the initial phase, distributed deformation produced short, unconnected thrusts; further fore-thrusts were generated successively at the toe of the wedge, with equal thrust widths in front of the FI. A single back-thrust, located near the indenter, initiated in the early phase and was active during the whole experiment, generating a deformable indenter (Fig. 5). All other thrusts were fore-thrusts. The wedge in front of the FI established a convex front due to lateral material transport towards the SI foreland, the transition to the slow indenter front (transfer zone) curves from convex to concave, whereas the SI wedge front is nearly straight (Figs. 6 and 8). At the boundary of the FI to the SI, a sinistral strike-slip fault evolves, normal to the indenter front, across the back-thrust part of the wedge (Fig. 7). Specific features of each experiment are:

- 40% experiment. The wedge in front of the FI and SI decouples after 7.5 cm FI convergence, further thrusting occurs independently in front of both indenters (Figs. 8 and 9).
- 50% experiment. The last connected thrust forms after 16 cm FI convergence; both wedges develop independently of each other thereafter. Further thrusts initiated at the FI front alternatingly die out in the transfer zone (different deformation than frontal thrusting - see Fig. 11) or run from the FI front alongside the FI close to the SI front. Strike in the curved thrust region has an angle of 70° to the indenter front.
- 55% experiment. Thrusts in front of the FI alternatingly propagate to the SI front or die out in the transfer zone. The last thrust, connecting both indenter fronts, develops after 43 cm FI convergence (Figs. 8 and 9). One further thrust becomes connected via the transfer zone, and the wedge front is strongly curved. An individual thrust with a strike-slip component occurs within the transfer zone.
- 60% experiment. The thrusts remain connected in front of the indenters during the whole experiment. However, some thrusts die out in the transfer zone and the thrust front becomes progressively curved in the course of the experiment.
- 70% experiment. The foreland wedge remains connected during the entire experimental run, and the wedge front is smoothly curved. Curvature increases during indentation; the transfer zone enlarges up to half of the SI width.
- 80% experiment. A smoothly curved wedge front develops early in the experiment and remains connected. Curvature increases during the experimental run and the transfer zone enlarges in front of the SI up to half width.

In summary, the maximum angle between the strike of the thrusts and the indenter front decreases from 70° in the 50% experiment to 20° in the 80% experiment (Figs. 7 and 8). In the experiments with a velocity ratio below 55%, the wedge decouples in an early stage. In experiments with velocity ratios of 55 to 60%, the wedges keep connected over a long period with partly independent thrusts and strongly curved thrust front, whereas in experiments with a velocity ratio of 70–80%, a smoothly curved thrust wedge evolves (Figs. 8 and 9).

3.1.2. Lateral material transport and rotation in the transfer zone

The 3D-displacement field obtained from particle image velocimetry is used to visualize oblique deformation relative to the indenter movement. Fig. 9 displays this portion of motion, normal to indentation, for all experiments of the first series, for each 10 cm of FI convergence. A large transfer zone evolves in the 60%, 70% and 80% experiments with oblique material transport towards to the SI foreland occurs. This oblique trusting, contempo-

Table 3
Parameters used in the experimental series: indenter speed, relative indenter velocity, and materials. FI, in front of the fast indenter; SI, in front of the slow indenter

Experiments		Relative velocity (%)	Velocity of fast indenter (cm/h)	Velocity of slow indenter (cm/h)	Thickness of glass beads (mm)	Thickness of silicone oil (mm)	Thickness of quartz sand (mm)
First series	gb40	40	120	48	3	-	15
	gb50	50	120	60	3	-	15
	gb55	55	120	66	3	-	15
	gb60	60	120	72	3	-	15
	gb70	70	120	84	3	-	15
	gb80	80	120	96	3	-	15
Second series	si60	60	2	1.2	-	5	15
	si-gb60	60	2	1.2	5 FI	5 SI	15

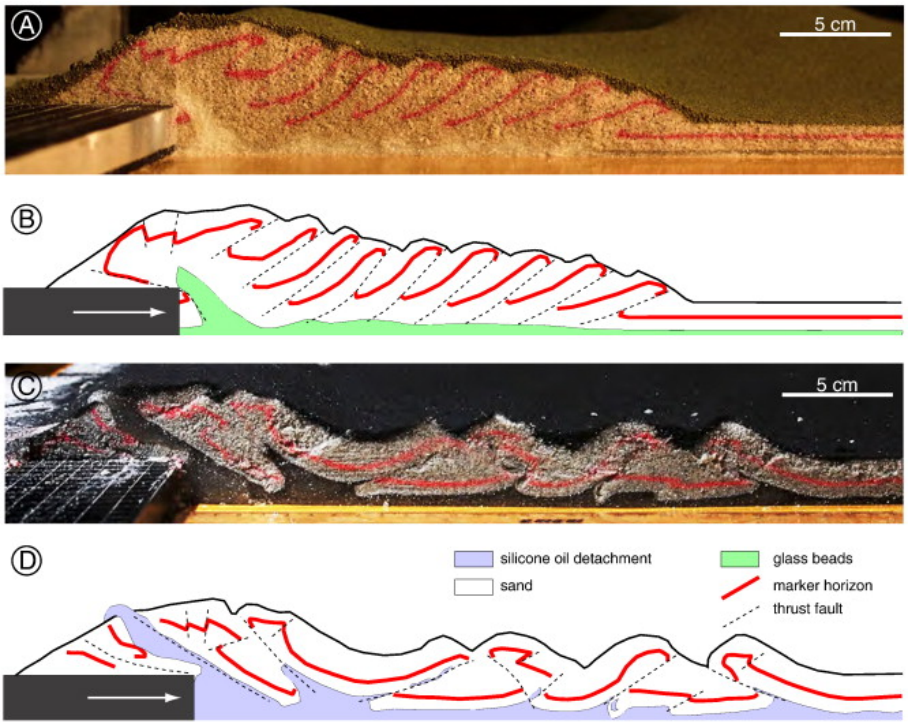

Figure 5. Cross-sections of the wedge in front of the slow indenter in the experiments with glass beads (gb) and silicone oil (si) as detachment horizon and with a relative velocity of 60% (the slow indenter moves with a relative velocity of 60% of the fast one). Picture (A) and the sketch (B) of the experiment gb 60 display regular fore-thrusting. Picture (C) and sketch (D) of experiment si60 show a wider and flatter wedge with fore- and back-thrusts.

raneous with wrenching in the transfer zone generates a counter-clockwise rotation in the transfer zone, with the highest amount of rotation close to the indenter (Fig. 10).

3.1.3. *Lateral thrust propagation*

As long as the thrust wedge in front of both indenters is connected, some or all thrusts nucleate at the toe of the FI front. Lateral propagation of a single thrust from initiation in front of the FI to the outermost part of the SI foreland needs up to 7 cm FI convergence. Thrusting is nearly independent in front of the SI in the experiments with large velocity contrast (40% and 50% experiments). The SI wedge becomes increasingly influenced by lateral thrust propagation from the FI with decreasing velocity contrast (55% and 60% experiments). In the 55% experiment, three thrust fronts are active at the same time. At a velocity ratio of 70–80%, almost all thrusts propagate laterally from the FI toward the SI front.

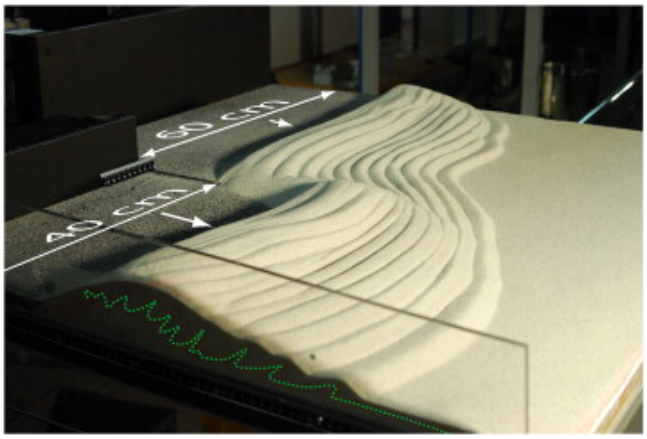

Figure 6. Oblique frontal view of the 70% experiment with a detachment made of glass beads at the final stage after 60 cm fast indenter convergence. A curved wedge developed in front of the fast (left in image) and the slow (rear in image) indenter which moved to the right front; green dashed line highlights the deformed passive marker horizon within the layer cake.

In all experiments, the region 25 cm to 35 cm away from the boundary between both indenters shows thrusts in the SI wedge without deflection. We used this region to measure the advance (spacing) of the deformation front at the moment of new thrust initiation (Figs. 11 and 13A). The 50% experiment has thrust spacings between 7.5 cm and 8 cm (Fig. 13B), which give the values for thrusts in front of the SI, not influenced by the FI wedge. The 55 and 60% experiments exhibit spacings between 5 and 8 cm, reflecting high variability in deformation-front advance; thrusts in front of the SI nucleate both in front of the SI and by lateral propagation from the FI front.

These velocity ratios are a transition from an independent SI wedge to an SI wedge controlled by the FI wedge. The 70 and 80% experiments exhibit thrusting in front of the SI that is significantly influenced by the FI thrust front characterised by 5 to 6 cm spacing with low standard deviation (Fig. 13B).

3.1.4. *Topography of the models in front of the two indenters*

Fig. 8 compiles the elevation evolution of the wedges in front of the indenters. The FI wedge becomes higher than the SI wedge due to greater shortening. The ridge crest has a lower elevation within the transfer zone than in front of the indenters due to extension along the strike of the transfer zone. We analysed the elevation increase of the SI wedge along the corridor unaffected by deflection caused by thrust–wedge interaction, i.e. 25 cm to 35 cm away from the boundary between both indenters (see above; Fig. 11). Then the highest point of the wedge (Fig. 13A) was plotted against SI convergence for many time steps (Fig. 13C). The self-affine growth of the wedge is a non-linear function of convergence. To eliminate thickness variation, we made a regression with a natural logarithmic (ln) function:

$$height = growth\ factor * ln(SI\ convergence) + b \quad (2)$$

SI wedge vertical growth is increasingly influenced by lateral thrust propagation at higher velocity ratios (40 to 60% experi-

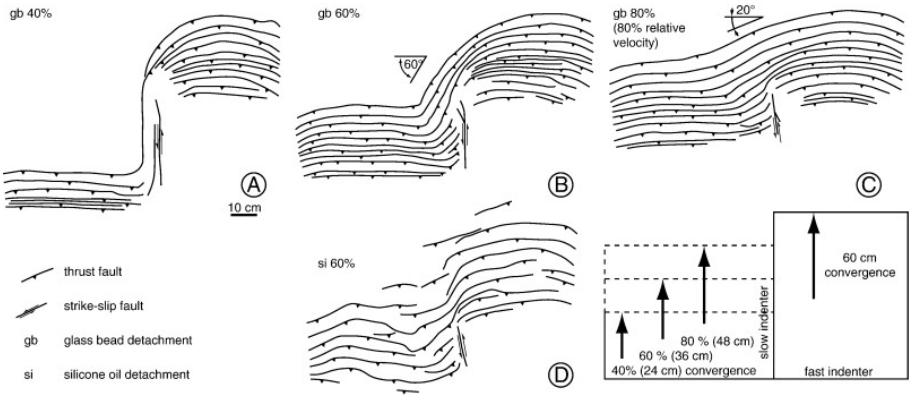

Figure 7. Line drawing of structures developed in the analogue-material experiments with glass beads detachment and relative velocity of 40, 60 and 80% (gb40, gb60, and bg80), highlighting the deformation style in the transfer zone (Fig. 11) between the two indenters. In the lower row, the silicone oil detachment experiment (si60) shows more irregular thrusting and a wider transfer zone. Bottom right: indenter sketch.

ments), reflected in decreasing growth factors (Fig. 13D). In experiments in which SI wedge growth is entirely influenced by lateral fault propagation (60 to 80% experiments) the increase in the growth factor depends on the relative velocity between the indenters, similar to the spacing between the thrusts.

3.2. *Second experiment series with a viscous silicone oil detachment*

The 60% experiment (gb60) with glass beads exhibits the most strongly curved continuous wedge in front of both indenters; it was chosen as our 'favourite' experiment (also in terms of reproducing some first-order features of our natural example, the Tajik basin; see below). Therefore, this velocity ratio was used to run an experiment (si60) with a detachment made of silicone oil. Our goal was to model the variation arising from the difference between brittle and viscous detachment rheologies. The growth of the wedge started with straight thrusts, whereas consecutive thrusts are more irregular and buckled than the gb60 experiment (Figs. 7, 12 and 15). The thrust front becomes slightly curved in the transfer zone and most thrusts propagate from the FI wedge to the SI front; irregular thrusts die out in the transfer zone as well as nucleate in the transfer zone or in the SI wedge front. Previously formed thrusts stay active even when newer thrusts are initiated at the toe of the wedge (Fig. 14). The final stage of the wedge after 60 cm convergence has a slightly curved thrust front with an internally deformed wedge (Fig. 7); the wedge has a lower slope angle than the wedge on top of the glass bead décollement. The dip direction of thrust is irregular with both fore- and back-thrusts (Fig. 5).

In another experiment, we introduced a lateral variation in weak layer rheology using glass beads and silicone oil. This 60% experiment (si-gb60) had a basal layer consisting of silicone oil in front of the SI and one comprising glass beads in front of the FI; both detachment materials had a thickness of 5 mm (Fig. 14 top). The experiment started with a few straight thrusts, which were alternatingly generated in front of both indenters or in the transfer zone. In an advanced stage, thrusts initiate at the FI front and propagate across the different detachment materials. The thrust front is nearly straight and less advanced in front of the FI than the SI (Figs. 12 and 15),

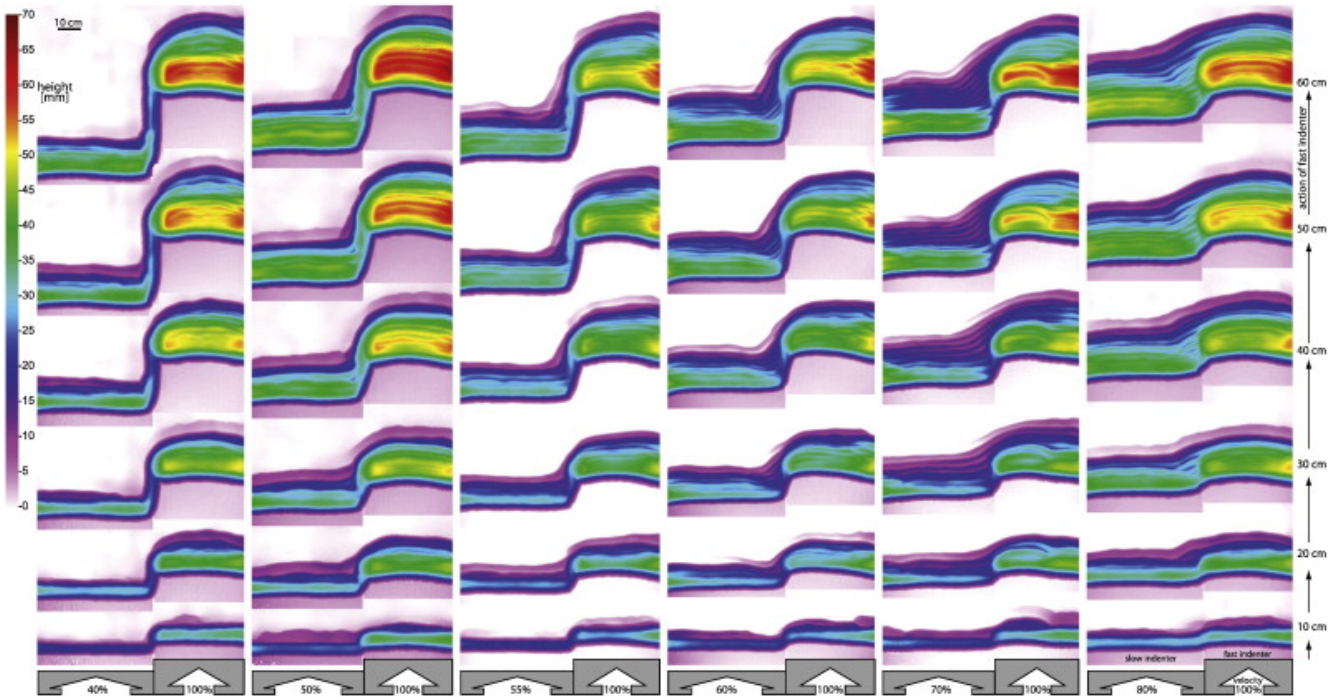

Figure 8. Overview of the surface-elevation development in all experiments with glass beads detachment after 10, 20, 30, 40, 50, and 60 cm convergence of the fast indenter. The wedge in front of both indenters remains connected during the experimental run or decouples depending on relative velocity and absolute convergence. Integrated wedges display onset and development of the curved wedge, with increasing curvature, in the transfer zone.

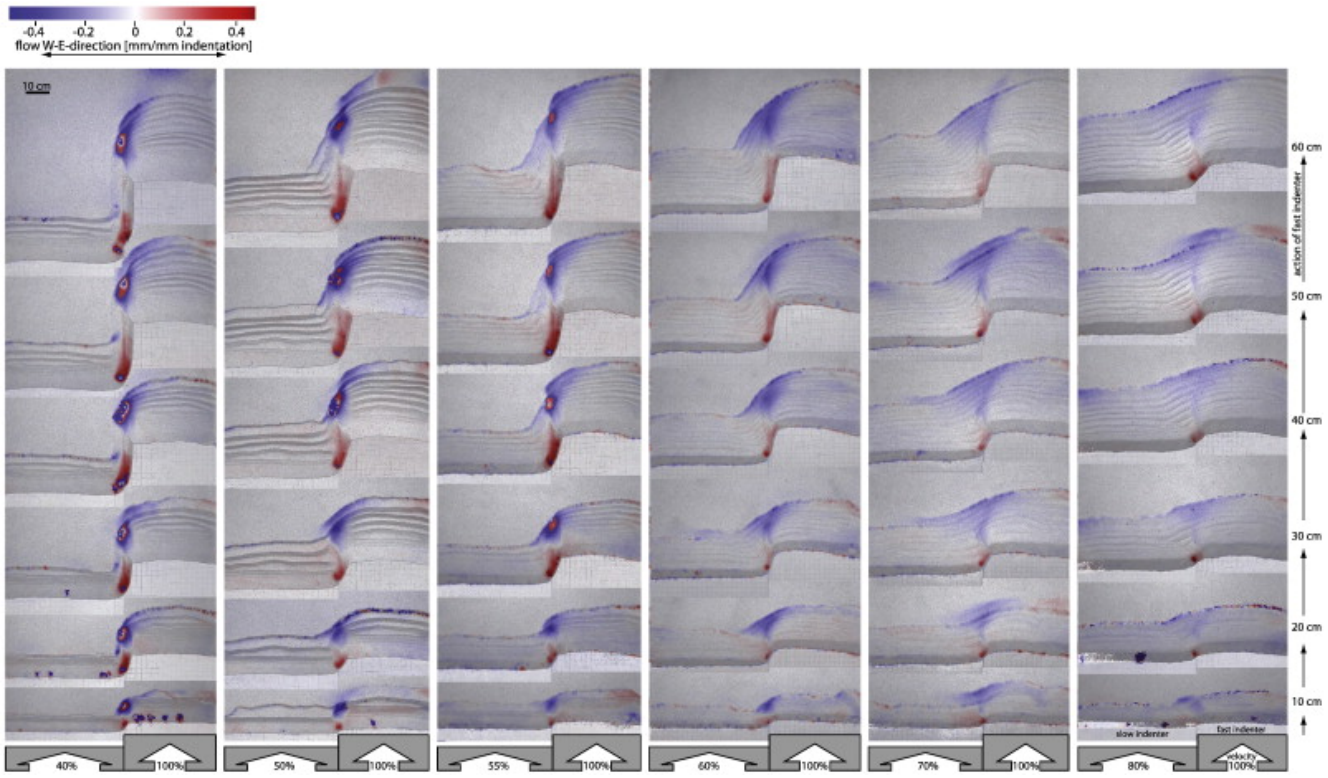

Figure 10. Overview of colour-coded portion of lateral material transport, perpendicular to the indentation direction, for all experiments, every 10 cm of fast indenter convergence. Especially the 60 and 70% experiments display a large area with oblique material transport in the transfer zone. Oblique thrusting, up to 70° relative to the indenter front, is also observed in disconnected frontal thrusts in the 50 and 55% experiments.

reflecting a larger slope angle due to the higher basal friction in the FI wedge. The si-gb60 experiment displays variable thrust geometries due to the contrasting décollement rheologies. Only fore-thrusts developed in the FI wedge (glass beads), but fore-and back-thrusts occurs in the SI wedge (silicone oil). The last two through-going thrusts in front of both indenters are connected at the surface but one thrust is a fore-thrust above the glass beads and a back-thrust above the silicon oil (Fig. 14 bottom). Earlier formed thrusts with different vergence are connected by splay faults.

4. Discussion

4.1. *Deformation of the experimental wedge in front of two indenters*

We designed an experimental set-up with two indenters moving in parallel and advancing with different velocities to

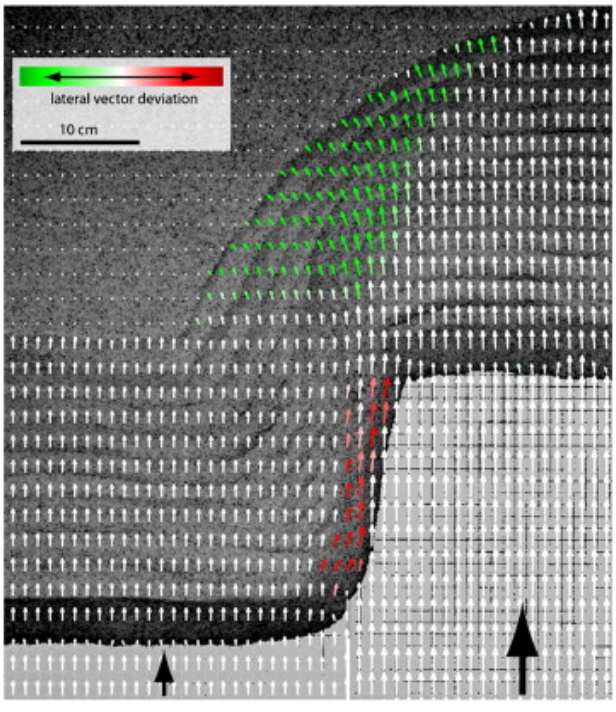

Figure 11. Counter-clockwise rotation in the transfer zone between the two indenters. Displacement of particles is illustrated by vectors. Picture show the 60% experiment after 60 cm of fast indenter convergence.

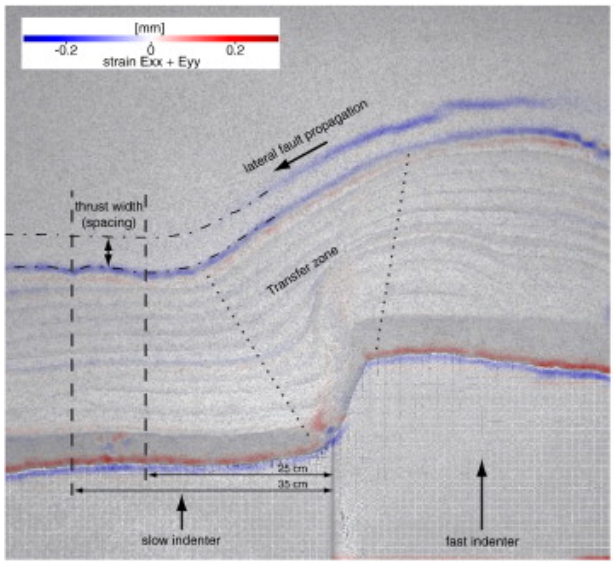

Figure 9. View from above onto the 70% experiment (gb70) after 50 cm of fast indenter convergence. Blue and red colours indicate active strain accommodation. Thrust spacing was measured (Fig. 13A and B) in a region without curvature (between the dashed lines) of the slow indenter wedge (25–35 cm from the border between the indenters). The transfer zone between the fast and the slow indenter is indicated by dotted lines, which displays more variable deformation than just frontal thrusting. Lateral fault propagation from the fast indenting wedge-part to the slow indenting wedge-part is indicated by an arrow.

model the evolution of a curved FTB in 3D. We tried to build a set-up with as few as possible boundary conditions to figure out the main effects (Fig. 4). We used flat indenters (*Bonini et al.*, 1999; *Byrne et al.*, 1988; *Koons*, 1990; *Persson and Sokoutis*, 2002; *Persson et al.*, 2004), which produce a deformable wedge with fore-thrusts and one long-living back-thrust along the indenter. This deformation style is similar to models of bivergent orogens (*Beaumont et al.*, 1996; *Malavieille*, 1984; *Silver and Reed*, 1988; *Willett et al.*, 1993) and a good analogue for continental collision orogeny at crustal scale.

In experiments with relative velocities above 55% (i.e. the slow indenter (SI) moves with a relative velocity greater than 55% of the fast one - FI), a continuous thrust wedge developed in front of both indenters. The velocity ratio influenced the bending of the wedge: In experiments with a low ratio, the wedge decoupled at an early stage; both wedges developed independently (Figs. 7 and 8). Velocity contrasts between both indenters were accommodated within the wedge by wrenching and/or a single strike-slip fault (with splay faults), subparallel to the indentation direction, running from the top of the wedge to the boundary between the indenters (Fig. 7).

In experiments with a velocity ratio > 55%, thrusting at the toe of the SI wedge is initiated by lateral propagation of thrusts from the FI wedge. Such a thrust wedge in front of the SI, influenced by lateral fault propagation, grows faster in width, is slower in elevation growth, and has a smaller slope angle than one without lateral fault propagation. This implies that thrust mechanics could be controlled along strike of up to 300 km or more in nature.

The vertical growth factor, calculated by regression with the natural logarithm (vertical wedge height versus convergence), allows estimation of self-controlling versus forced SI wedge growth. A growth factor > 1 characterizes independent SI wedge growth, whereas a growth factor < 1 describes an SI wedge influenced by FI growth. The experiments show that thrust nucleation spacing and the vertical growth factor are a linear function of the velocity ratio (Fig. 13B and D) as long as the entire wedge in front of both indenters remains connected (> 60%).

Furthermore, lateral fault propagation forces a difference of deformation within the SI wedge. To initiate a new thrust, peak strength (which is equivalent to peak friction) has to be overcome (*Gutscher et al.*, 1998); however, when a fault propagates laterally, the stress at the tip of the rupture is higher, which makes lateral propagation of the thrust more favourable. In accordance with the minimum work concept (*Masek and Duncan*, 1998), lateral thrust propagation requires less work than thrust initiation, which lowers taper angles similar to a lower internal or basal friction. This explains why there is an equal number of thrusts in front of the SI and FI as long as the entire wedge remains connected and the SI wedge grows more slowly.

Lateral thrust propagation occurs over a width of more than 60 cm in the experiments with a velocity ratio larger than 55%; this would be more than 300 km in nature. As the lateral propagation of thrusts is active over ≈7 cm (≈35 km in nature) FI convergence, lateral thrust propagation over a distance of 300 km would last ≈3 Myr; the thrust in nature would propagate laterally at ≈10 cm/yr, whereas frontal convergence would be ≈1 cm/yr (Table 4). A thrust cycle of ≈3 Myr duration at a basement depth of ≈8 km is similar to that observed in the Apennines and Subandean belts (*Hoth et al.*, 2007).

Cooper et al. (2003) compared propagation rates of thrusts in (straight) foreland fold-and-thrust belts: They found lateral fault-propagation rates in the range of 0.1–3 cm/yr and uplift/shortening rates between 0.01 and 0.44 cm/yr, in the same order of magnitude as we derived from our experiments, if scaled to nature (Table 4). Furthermore, a velocity ratio of ≈0.1 between maximum displacement and maximum along strike length of a thrust determined by *Cooper et al.* (2003) compares well to our results; this comparison suggests that extrapolation of the experimental results to nature is reliable when proper scaling is used.

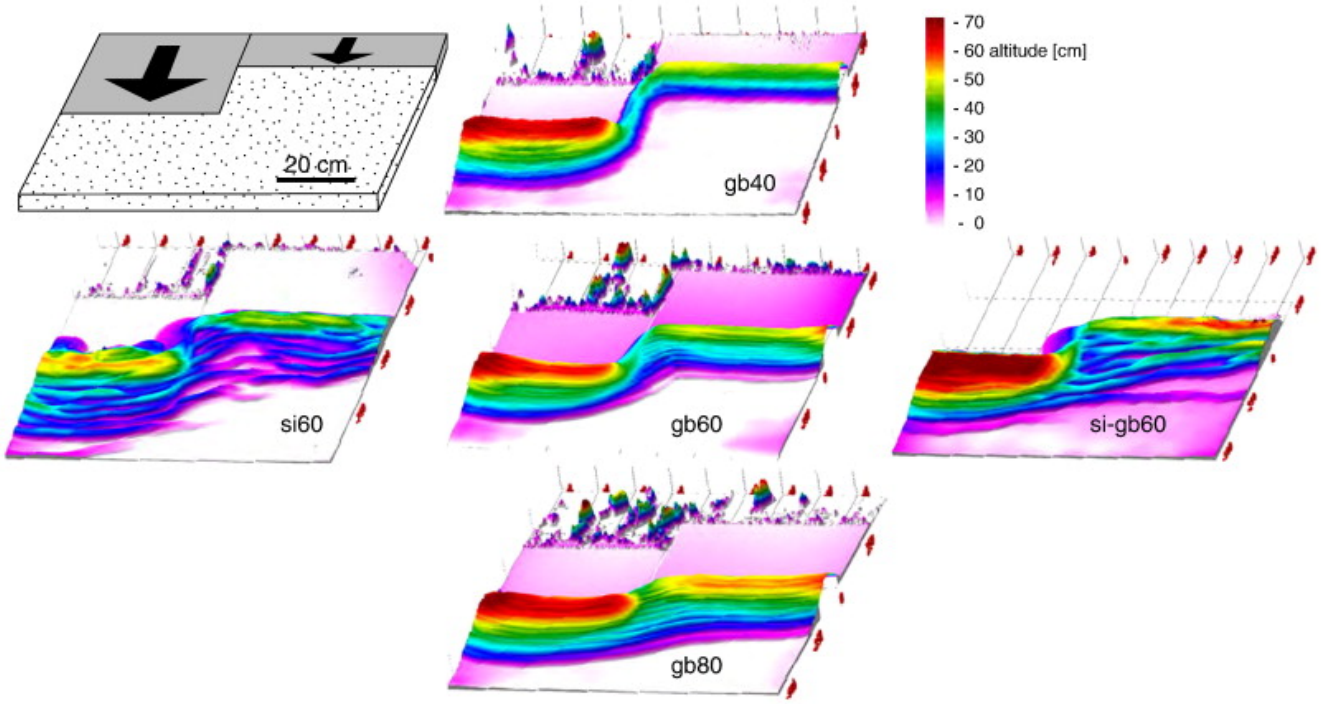

Figure 12. Thrust wedges in 3D view in the final stage after 60 cm fast indenter convergence of the 40% (gb40), 60% (gb60), and 80% (gb80) experiments with glass beads detachment. The wedge of the 40% experiment decouples in an early stage. The 60% (gb60) model wedge is connected but strongly curved, whereas the 80% experiment has a smoothly curved wedge. The experiments with 60% relative velocity and the detachment made of silicone oil (si60) or of glass beads in front of the fast indenter and the silicone oil in front of the slow indenter (si-gb60) display the influence of the detachment rheology on the surface deformation. The length of a wedge is about 100 cm, the surface is colour coded according to height. The steep topography behind the indenters is an artefact of lost optical correlation. Set-up sketch is in the upper left corner.

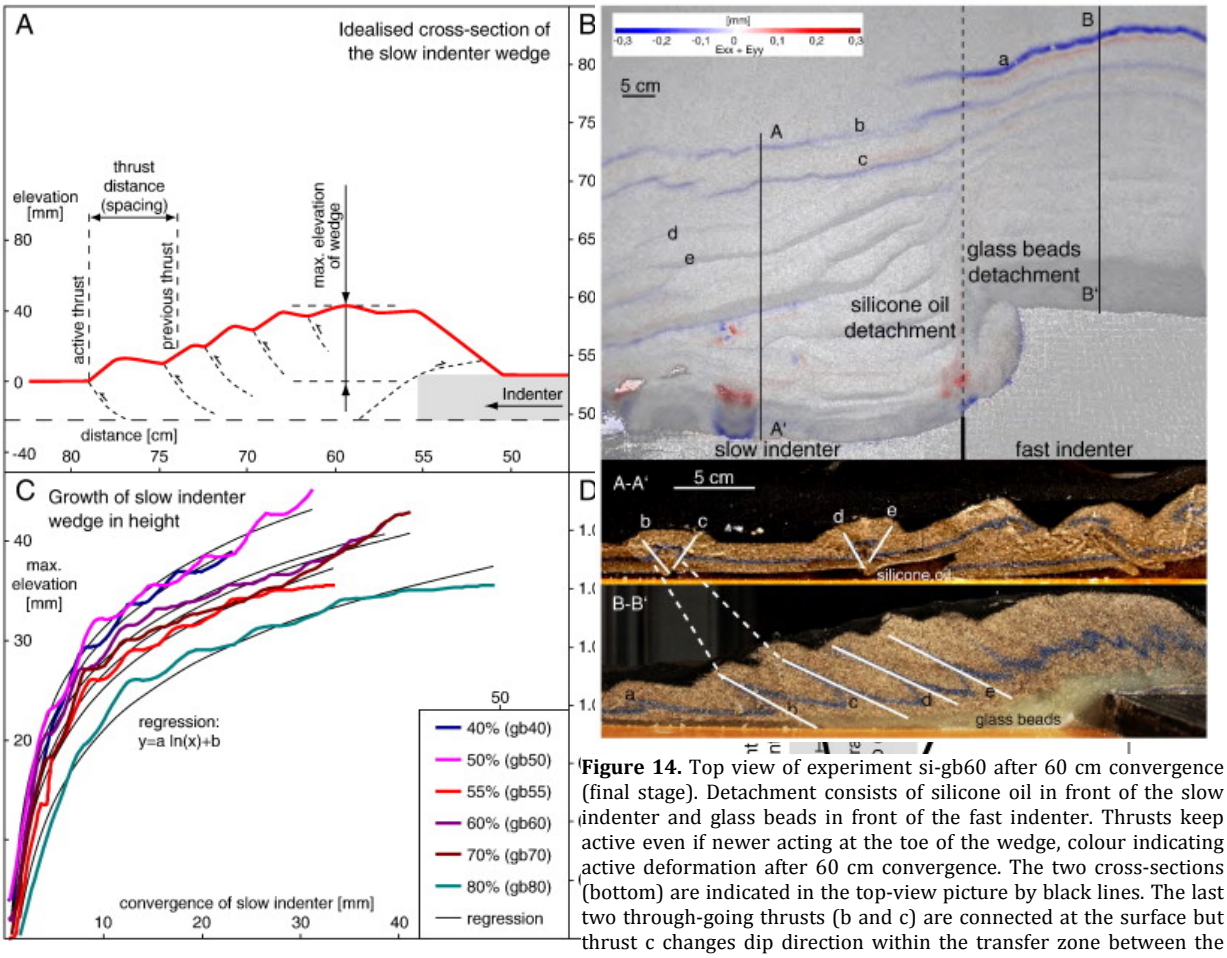

Figure 13. A) Schematic cross-section of the slow indenter (SI) wedge in t of 55% of the fast one; the experiment has a glass beads detachment layer) after 55 cm fast indenter (FI) convergence in an undeformed region (Fig. 11) outside of the transfer zone between the indenters. B) Thrust widths are measured in front of the SI in an undeformed region (Fig. 11 and subfigure A) outside of the transfer zone between the indenters. Box plots display the thrust widths, median in red, lower and upper quantile indicated by the blue boxes, standard deviation by the whiskers. C) Growth of the SI wedge in height versus convergence of the SI for all glass beads experiments, including regression. D) Logarithmic factor (ln) of SI wedge growth (subfigure C) versus relative velocity ratios. A low value represents a slowly growing wedge under identical convergence rate. Lateral fault propagation increases growth in wedge width and consequently decreases growth in height. Standard deviation is displayed by bars. The grey vertical bar indicates velocity ratios with independent, transition from independent to controlled and controlled SI wedge grow/thrusting, affected by the FI wedge.

Figure 14. Top view of experiment si-gb60 after 60 cm convergence (final stage). Detachment consists of silicone oil in front of the slow indenter and glass beads in front of the fast indenter. Thrusts keep active even if newer acting at the toe of the wedge, colour indicating active deformation after 60 cm convergence. The two cross-sections (bottom) are indicated in the top-view picture by black lines. The last two through-going thrusts (b and c) are connected at the surface but thrust c changes dip direction within the transfer zone between the two indenters.

Our second experimental series tested the influence of décollement rheology. The viscous detachment lowered the slope angle of the wedge and allowed for varying thrust vergence and long-lasting thrust activity (*Costa and Vendeville*, 2002; *Couzens-Schultz et al.*, 2003; *Davis and Engelder*, 1985). The silicone oil and glass beads (si-gb60) experiment displayed different thrust geometries depending on the detachment rheology: fore-thrusting atop of the glass beads and varying thrust vergence above the silicone oil; one thrust is connected on the surface but displays different vergence within the wedge, being a fore-thrust above the glass beads and a back-thrust above the silicone oil. This indicates that lateral thrust propagation initiated close to the surface and propagated down to the detachment (Figs. 14 and 15).

Previous analogue experiments (*Calassou et al.*, 1993; *Costa and Vendeville*, 2002; *Cotton and Koyi*, 2000; *Couzens-Schultz et al.*, 2003; *Keep*, 2000; *Macedo and Marshak*, 1999; *Marques and Cobbold*, 2002, 2006; *Marshak*, 2004; *Marshak and Wilkerson*, 1992; *Schreurs et al.*, 2001; *Zweigel*, 1998) investigated, which parameters may control the evolution of a curved FTB. These parameters are lateral thickness variations of the sedimentary basin fill, indenter shape, detachment rheology and its lateral changes and foreland width. Our set-up with two adjacent indenters, moving in parallel with a given relative velocity is a new parameter (or a time depending variation of indenter shape).

The smoothly curved indenter used in one experiment of *Macedo and Marshak* (1999) generated curved thrusts oblique to the indentation; obliquity decreased with further indentation. This is in contrast to our model, where obliquity and bending increase during indentation. A decrease in curvature during indentation is also observed in the experiments of *Calassou et al.* (1993), where the indenter front becomes smoother during progressive wedge accretion. *Zweigel* (1998) used a rhombohedric indenter to create an arcuate thrust wedge; thrusting up to 70° oblique to the indentation direction was observed, but thrusts tore at the leading edge. All these experiments exhibit rotation at the edge of the indenter and decreasing bending during indentation (see also *Marques and Cobbold*, 2002, 2006). Curvature increases only in experiments with a lateral variation in thickness or basal friction (*Calassou et al.*, 1993; *Macedo and Marshak*, 1999). Our results, i.e. with thrust orientation and slope angle depending on the detachment rheology, agree with *Costa and Vendeville* (2002) and *Cotton and Koyi* (2000), producing a curved thrust front above a ductile to frictional detachment.

4.2. *Comparison of experimental results with the Tajik fold-and-thrust belt*

The Tajik basin is an intra-continental basin with a curved fold-and-thrust belt north of the Hindu-Kush and northwest of

the Pamir orocline. Its northern, straight and east-trending boundary is the Tien Shan (Fig. 1A and C). The Tajik basin is considered a classic FTB with a low-angle taper that developed along a basal detachment of Jurassic evaporites (*Bekker*, 1996; *Burtman and Molnar*, 1993; *Hamburger et al.*, 1992; *Keith et al.*, 1982; *Leith and Alvarez*, 1985). The deformation field determined by GPS-geodesy (*Mohadjer et al.*, 2010; *Reigber et al.*, 2001) and seismicity (Fig. 1B; *Burtman and Molnar*, 1993) suggests that the Pamir and the Hindu-Kush act as indenters and the Tien Shan as an obstacle (Fig. 1C).

Deformation within the Tajik basin has been accommodated by northwest-ward displacement of the basin fill between a dextral thrust zone along the Tien Shan to the north and a sinistral thrust zone within Afghanistan to the south. Furthermore, deformation occurred by thrusting along north-east-trending ranges within the basin, counter-clockwise block rotations, and intra-continental subduction along the Pamir front (Fig. 1C; *Hamburger et al.*, 1992; *Leith and Alvarez*, 1985; *Thomas et al.*, 1994a, b, 1996). Seismicity suggested active intra-continental subduction along Hindu-Kush and the Pamir front (*Billington et al.*, 1977; *Chatelain et al.*, 1980; *Negredo et al.*, 2007; *Roecker et al.*, 1980).

Bourgeois et al. (1997) restored deformation pattern within the Tajik basin, suggesting a rotated indenter whereas *Leith and Alvarez* (1985) suggest that the Tajik FTB is pressed against the slope of the Gissar Range. *Brookfield and Hashmat* (2001) suggest that westward directed gravitational gliding of the fold-and-thrust belt might be triggered by the northward movement of the Pamir. Using the classification of Macedo *and Marshak* (1999), basin controlled vs. indenter controlled, the Tajik basin would be classified as an indenter controlled basin, because trend lines converges at the apex of the salient, which is to find in the north of the Pamir. However, this part of the FTB is now strongly squeezed between the Pamir and the Tien Shan. In contrast curvature of the Tajik FTB was increased during deformation, which would be a typical feature of basin controlled salients. However, Pamir indentation separated the former Touran Sea with the eastern shoreline about 600–700 km further to the east, into the Tajik and Tarim basin (*Bally et al.*, 1986 cited in *Burtman*, 2000; *Hamburger et al.*, 1992; *Sobel*, 1999).

In our experiments, we used geometric and physical properties similar to the setting of the Tajik basin. In the following, we compare the experimental results with the overall geologic structures of the Tajik FTB.

- Our study suggests that a curved FTB develops when two neighbouring blocks penetrate into a foreland basin with different velocities, but with a low velocity contrast. The curved thrust wedge in the 60% experiment shows principle geometric similarities with the Tajik FTB (Figs. 1C and 7), being convex on the northwest side of the FI, the Pamir.
- Counter-clockwise rotation has been reported within the Tajik basin, with the largest amounts close to the Pamir (*Bazhenov and Burtman*, 1986; *Bazhenov et al.*, 1994; *Thomas et al.*, 1994a). Our experimental results show similar counter-clockwise rotations in the transfer zone, close to the FI. This illustrates that the indenter itself does not necessarily need to rotate (*Bourgeois et al.*, 1997) to generate rotations like those observed in the Tajik basin.

Table 4
Comparison between our velocities of thrust activity scaled to nature and thrust velocities in nature (long-term average).

	Velocity scaled to nature (cm/yr)	Velocity in nature (cm/yr)
Lateral thrust propagation	10	0.1–3[a]
Frontal thrusting	1	0.01–0.44[a]

[a] Cooper et al. (2003).

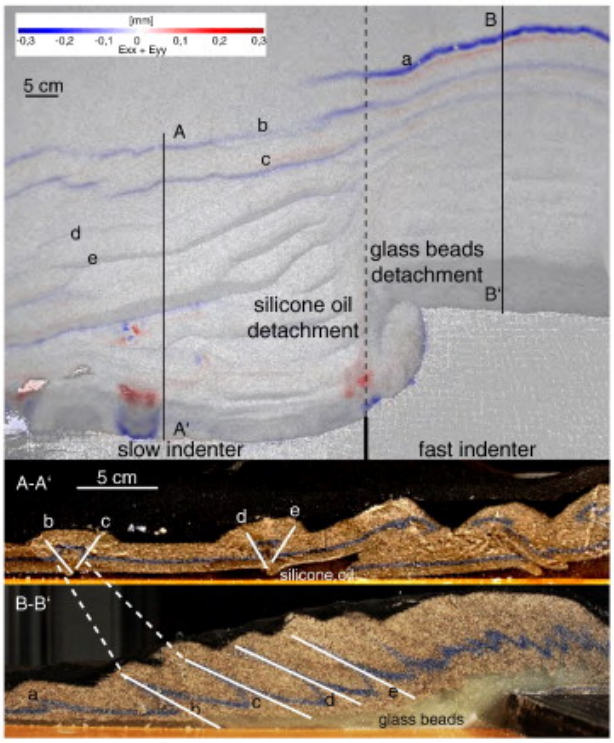

Figure 15. Top view of experiment si-gb60 after 60 cm convergence (final stage). Detachment consists of silicone oil in front of the slow indenter and glass beads in front of the fast indenter. Thrusts keep active even if newer acting at the toe of the wedge, colour indicating active deformation after 60 cm convergence. The two cross-sections (bottom) are indicated in the top-view picture by black lines. The last two through-going thrusts (b and c) are connected at the surface but thrust c changes dip direction within the transfer zone between the two indenters.

- Our model suggested convergence between Hindu-Kush and Tien Shan at a ratio of 60% of Pamir–Tien Shan convergence. Shortening between the southern Pamir and the Tien Shan are in the range of ≈600 km (e.g. *Burtman and Molnar*, 1993) this equates to ≈360 km shortening between southern Hindu Kush and Tien Shan, accommodated within the Tajik basin and the Hindu Kush.
- At the current stage of mapping, the front of the Hindu-Kush in the Tajik basin does not show a well-developed east- or east-north-east-striking FTB, as observed in the analogue experiments. It was suggested that the sediment stack in the Tajik basin has a prismatic shape and becomes thicker to the south, due to the protrusion of the Pamir and the Hindu-Kush (*Leith*, 1982). Besides the poor knowledge of the southern Tajik basin, one explanation for the apparent absence of a FTB at the southern margin of the basin might be that it is covered by thick Quaternary deposits (*Schwab et al.*, 1980; *Thomas et al.*, 1994a). As the drainage systems merge and the major trunk stream (the Amu Darya) is located in the southern Tajik basin, the thickest Quaternary deposits accumulated there. According to the critical taper theory, thrusting occurs in front of the evolving wedge; in this manner, the low angle prismatic basin infill in the southern Tajik basin may reflect a part of the currently inactive inner wedge, similar to that has been observed in numerical and analogue models (*Simpson*, 2010; *Smit et al.*, 2010). Structural field work and denser surface deformation monitoring would be necessary to test this hypothesis.
- Cross-sections (Fig. 16; *Bekker*, 1996; *Bourgeois et al.*, 1997; *Thomas et al.*, 1994a) indicate that folds and thrusts verge north-west in the eastern part of the Tajik basin and south-east in its western part (Fig. 16, cross-section C–C′); this suggests a vergence toward to the centre of the basin. The thrust front along the northern margin of the Pamir is exclusively

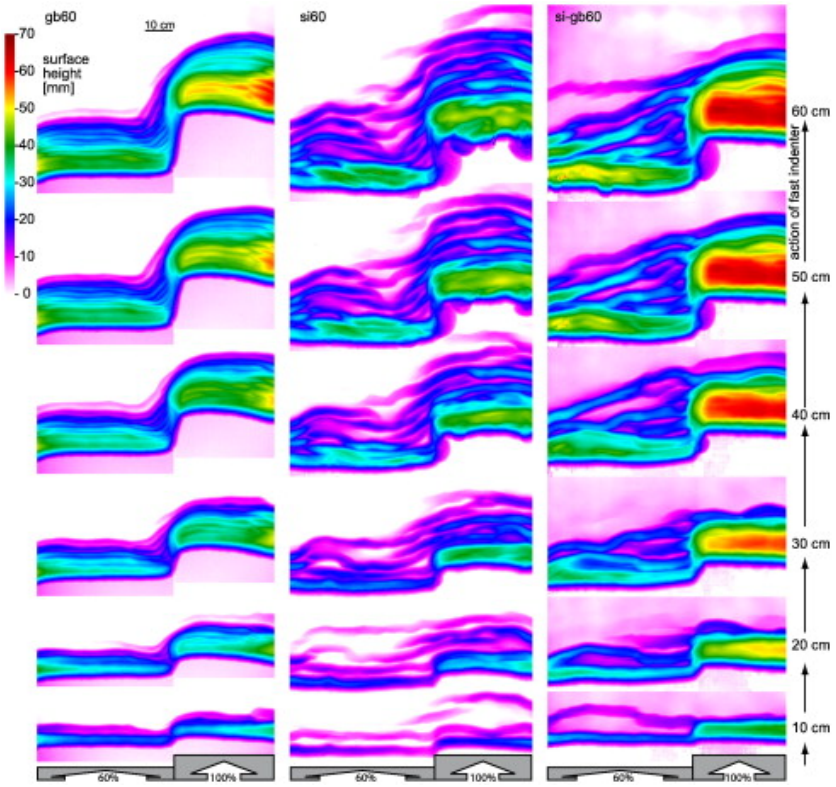

Figure 16. Comparison of the elevation of the 60% experiments with the glass beads detachment (gb60), silicone oil detachment (si60), and the detachment (si-gb60) with silicone oil in front of the slow indenter (SI) and glass beads in front of the fast indenter (FI). The development of the surface is illustrated after each 10 cm advance of the FI. Indenters are displayed by grey boxes with the FI on the right and the SI on the left side.

north vergent (Fig. 16, cross-sections A–A′ and B–B′; *Bekker*, 1996; *Leith and Alvarez*, 1985). In our experiment with a changing detachment rheology (si-gb60), fore- and back-thrusting developed along the viscous detachment and fore-thrusts along the brittle detachment; this is similar to the Tajik basin that is underlain by Jurassic salt that becomes discontinuous and dies out eastward (e.g. *Vlasov et al.*, 1991).

- The north-eastern front of the Tajik FTB, its connection with the Tarim basin, is tightly squeezed between the Pamir and the Tien Shan. In our experiments, such a pattern is not observed, as we did not incorporate a rigid hinterland in the set-up.

4.3. *Application of the two indenter model to the Sulaiman Range*

The Sulaiman Range of Pakistan is an arcuate FTB (Fig. 17) which has evolved since the Paleocene (*Farah et al.*, 1984). Currently the Sulaiman Range accommodates 5–14 mm of north–south shortening between India and Eurasia and 3-6 mm of east–west shortening (*Bernard et al.*, 2000). Further west, the north–south oriented Chaman fault absorbs large left-lateral strike-slip displacement. During the development of the FTB different stratigraphic detachments have been connected by ramps as well as thickness variations of the sedimentary pile are presumed (*Davis and Lillie*, 1994; *Humayon et al.*, 1991). The occurrence of a weak detachment layer, like evaporates, is suggested by the small overall taper of the Sulaiman wedge, but no outcrop of the décollement layer has been detected (*Davis and Lillie*, 1994). However, the topographic relief is more impressive close to the front in the south and in the eastern part of the FTB. The Sulaiman FTB is highly oblique in the eastern part to the overall transport direction of the Sulaiman lobe (*Humayon et al.*, 1991). Orientations of the structures ranges from parallel up to normal in relation to the plate convergence (north–south) around the salient (*Haq and Davis*, 1997; *Macedo and Marshak*, 1999).

Haq and Davis (1997) studied the deformation pattern generated due to a separated tectonic block (Katawaz block), squeezed between India and Afghanistan. The curvature of the FTB suggests the Sulaiman Range to be either a typical basin controlled salient (*Macedo and Marshak*, 1999), caused by lateral variation of the depth to the detachment (Fig. 17), or a salient associated with along-strike heterogeneities in basal mechanical coupling (*Davis and Lillie*, 1994). The separation of the FTB structures and the occurrence of strike-slip faults as transfer zones could be explained by oblique indentation of a smooth curving indenter (*Macedo and Marshak*, 1999). But the toe of the wedge in the middle, advanced part of the salient (Fig. 17) is still on top of the deepest sediment pile. This depth

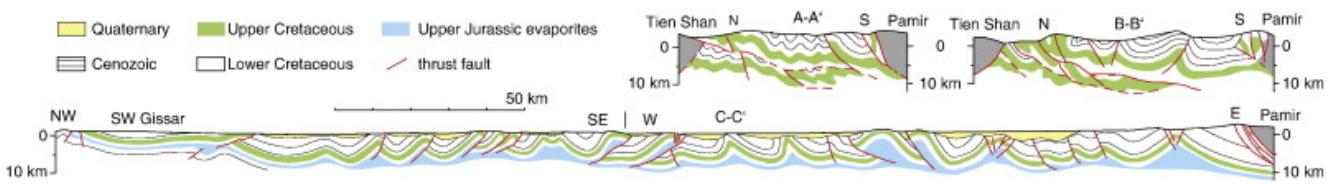

Figure 17. Cross-sections of the Tajik basin, in the north eastern part (A–A′ and B–B′), redrawn after Bekker (1996), illustrating north and north-westward folding and thrusting. The west–east oriented cross-section across the Tajik basin (C–C′) exhibit orientation to the centre of the basin (redrawn after *Bourgeois et al.* (1997), based on VNIGNI data). Section lines are indicated in Fig. 1.

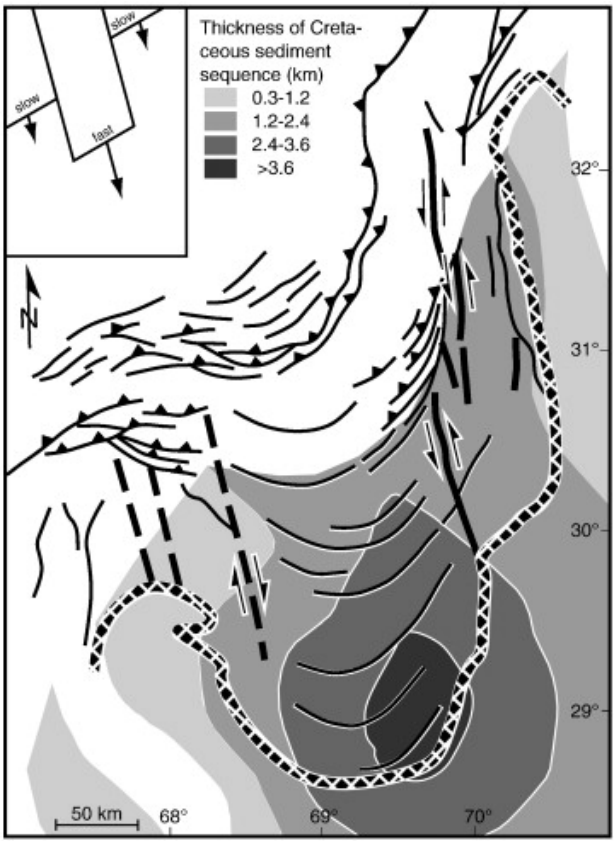

Figure 18. Simplified tectonic map of the Sulaiman Range (Pakistan), modified after *Macedo and Marshak* (1999). Shaded regions illustrate the thickness distribution of a Cretaceous sequence, below the intense curved fold-and-thrust belt. The toe of the advanced part of the wedge is still above the deepest part of the sedimentary sequence. The inset-sketch illustrates the hypothetically acting three indenters with different velocities, moving in parallel.

variation below the thrust front could influence the curvature of the salient presumably only minor. More important is the deepness variation of the acting indenter, which is not pronounced. Structures in the Sulaiman Range are in general curved, like the thrusts in the north-western part, on top of the wedge. The deformation pattern of the Sulaiman Range is influenced by the thickness distribution of the sediments and the different mechanical properties of the detachment in any case. However, these structures are also to explain by the deformation and fallowed decoupling of the wedge in front of two or more indenters.

The south-eastern part of the Sulaiman Range exhibits a sinistral strike slip fault, striking normal to the overall plate-tectonic convergence, a feature which is observed in our experiments with the glass beads décollement and velocity ratio of ≈55%, between the fast and the slow indenter. The sequential highly oblique thrusting in the Sulaiman Range is a feature which is also to observe in our experiments. We suggest that the deformation pattern in the Sulaiman Range could be generated by considering two or more indenters advancing at different velocities. For instance the sketch in Fig. 17 illustrates a re-interpretation involving three oblique indenters. The decoupling of the FTBs and the occurrence of strike-slip transfer faults in the eastern part may indicate a large difference in indentation velocity.

5. Conclusions

To study the formation of curved FTBs, a new experimental set-up with two adjacent parallel moving indenters with different velocity ratios was used. It generates curved thrust-and-fold wedges characterized by oblique thrusting, material rotation, oblique material transport, and lateral thrust propagation. 3D particle-image velocimetry observations allow the quantification of the model topography, the analysis of thrust distances and wedge growth. In a first experimental series, we investigated the influence of velocity contrast between the indenters on the bending of the wedge(s). Accordingly, bending increase during indentation. The wedge remains connected at low velocity contrasts (ratios > 55%), and disconnects when velocity contrast is high (≤ 55%). Furthermore, the experiments featured rotation and oblique thrusting as well as material transport in the transfer zone between the two indenter wedges. Lateral thrust propagation from the FI wedge to the SI wedge front forces the thrust spacing and height of the slow indenter wedge. This lateral thrust propagation exhibits a far field effect along strike of more than 300 km scaled to nature. Ratios of convergence to lateral thrust propagation rates at about 1/10 compare well with those estimated for natural FTBs. The experiment with 60% relative velocity (the slow indenter moves with a relative velocity of 60% of the fast one) and the glass beads décollement generated a wedge that shares most similarities with the Tajik basin FTB; e.g. curvature and most pronounced block rotations close to the Pamir indenter. A viscous décollement, studied in our second experimental series, enables an irregular thrust dip; this might explain the vergence of folds and thrusts towards the centre in the Tajik basin, which is suggested to be underlain by an evaporitic detachment.

Acknowledgements

The experiments of this study were carried out in the analogue laboratory of the German Research Centre for Geosciences GFZ in Potsdam. Partly funded by the "Freunde und Förderer der TU Bergakademie Freiberg" and the Deutsche Forschungsgemeinschaft in the frame work of the bundle 443 (TIPAGE, RA 442/35). Fig. 1 was largely done with GMT. We thank David Boutelier for measurements of the viscosity of the silicone oil used in this study as well as Matthias Rosenau and Silvan Hoth for helpful discussion. We also have to thank two anonymous reviewers for their constructive annotation, which improve the manuscript.

References

Adam, J., Urai, J.L., Wieneke, B., Oncken, O., Pfeiffer, K., Kukowski, N., Lohrmann, J., Hoth, S., van der Zee, W., Schmatz, J., 2005. Shear localisation and strain distribution during tectonic faulting -new insights from granular-flow experiments and high-resolution optical image correlation techniques. J. Struct. Geol. 27 (2), 283–301.

Arroyo, M.P., Greated, C.A., 1991. Stereoscopic particle image velocimetry. Meas. Sci. Technol. 2 (12), 1181–1186.

Bally, A.W., Chou, I.-M., Clayton, R., Eugster, H.P., Kidwell, S., Meckel, L.D., Ryder, R.T., Watts, A.B., Wilson, A.A., 1986. Notes on sedimentary basins in China; report of the American Sedimentary Basins Delegation to the People's Republic of China. Open-File Report - U. S. Geological Survey, Report: OF 86-0327. 108.

Bazhenov, M.L., Burtman, V.S., 1986. Tectonics and paleomagnetism of structural arcs of the Pamir–Punjab syntaxis. J. Geodyn. 5 (3–4), 383–396.

Bazhenov, M.L., Perroud, H., Chauvin, A., Burtman, V.S., Thomas, J.-C., 1994. Paleomagnetism of Cretaceous red beds from Tadzhikistan and Cenozoic deformation due to India–Eurasia collision. Earth Planet. Sci. Lett. 124 (1–4), 1–18.

Beaumont, C., Ellis, S., Hamilton, J., Fullsack, P., 1996. Mechanical model for subduction–collision tectonics of Alpine-type compressional orogens. Geology 24 (8), 675–678.

Bekker, Y.A., 1996. Tectonics of the Afghan–Tadshik Depression (russ.). Geotektonika 30 (1), 76–82.

Bernard, M., Shen-Tu, B., Holt, W.E., Davis, D.M., 2000. Kinematics of active deformation in the Sulaiman Lobe and Range, Pakistan. J. Geophys. Res. 105 (B6), 13,253–13,279.

Billington, S., Isacks, B.L., Barazangi, M., 1977. Spatial distribution and focal mechanisms of mantle earthquakes in the Hindu Kush–Pamir region: a contorted Benioff zone. Geology (Boulder) 5 (11), 699–704.
Bonini, M., Sokoutis, D., Talbot, C.J., Boccaletti, M., Milnes, A.G., 1999. Indenter growth in analogue models of Alpine-type deformation. Tectonics 18 (1), 119–128.
Bourgeois, O., Cobbold, P.R., Rouby, D., Thomas, J.-C., Shein, V., Shein, V., 1997. Least squares restoration of Tertiary thrust sheets in map view, Tajik Depression, Central Asia. J. Geophys. Res. 102 (B12), 27,553–27,573.
Brookfield, M., Hashmat, A., 2001. The geology and petroleum potential of the North Afghan platform and adjacent areas (northern Afghanistan, with parts of southern Turkmenistan, Uzbekistan and Tajikistan). Earth Sci. Rev. 55 (1–2), 41–71.
Burtman, V.S., 2000. Cenozoic crustal shortening between the Pamir and Tien Shan and a reconstruction of the Pamir–Tien Shan transition zone for the Cretaceous and Palaeogene. Tectonophysics 319 (2), 69–92.
Burtman, V.S., Molnar, P., 1993. Geological and geophysical evidence for deep subduction of continental crust beneath the Pamir. Geol. Soc. Am. Spec. Pap. 281, 1–76.
Byerlee, J., 1978. Friction of rocks. Pure Appl. Geophys. 116 (4–5), 615–626.
Byrne, D.E., Davis, D.M., Sykes, L.R., 1988. Loci and maximum size of thrust earthquakes and the mechanics of the shallow region of subduction zones. Tectonics 7 (4), 833–857.
Calassou, S., Larroque, C., Malavieille, J., 1993. Transfer zones of deformation in thrust wedges: an experimental study. Tectonophysics 221 (3–4), 325–344.
Chatelain, J.L., Roecker, S.W., Hatzfeld, D., Molnar, P., 1980. Microearthquake seismicity and fault plane solutions in the Hindu Kush region and their tectonic implications. J. Geophys. Res. 85 (B3), 1365–1387.
Chu, J., 1995. An experimental examination of the critical state and other similar concepts for granular soils. Can. Geotech. J. 32 (6), 1065–1075.
Clark, G.B., 1966. Deformation moduli of rocks. ASTM Spec. Tech. Publ. 402, 133–172.
Cooper, K.A., Hardy, S., Gawthorpe, R., 2003. Stratigraphic and structural expression of the lateral growth of thrust fault-propagation folds: results and implications from kinematic modelling. Basin Res. 15 (2), 165–182.
Costa, E., Vendeville, B.C., 2002. Experimental insights on the geometry and kinematics of fold-and-thrust belts above weak, viscous evaporitic décollement. J. Struct. Geol. 24 (11), 1729–1739.
Cotton, J.T., Koyi, H.A., 2000. Modeling of thrust fronts above ductile and frictional detachments: application to structures in the Salt Range and Potwar Plateau, Pakistan. Geol. Soc. Am. Bull. 112 (3), 351–363.
Coutand, I., Strecker, M.R., Arrowsmith, J.R., Hilley, G., Thiede, R.C., Korjenkov, A., Omuraliev, M., 2002. Late Cenozoic tectonic development of the intramontane Alai Valley, (Pamir–Tien Shan region, Central Asia): an example of intracontinental deformation due to the Indo-Eurasia collision. Tectonics 21 (6), 19.
Couzens-Schultz, B.A., Vendeville, B.C., Wiltschko, D.V., 2003. Duplex style and triangle zone formation: insights from physical modeling. J. Struct. Geol. 25 (10), 1623–1644.
Dahlen, F.A., Suppe, J., Davis, D., 1984. Mechanics of fold-and-thrust belts and accretionary wedges; cohesive Coulomb theory. J. Geophys. Res. 89 (B12), 10,087–10,101.
Davis, D.M., Engelder, T., 1985. The role of salt in fold-and-thrust belts. Tectonophysics 119 (1–4), 67–88.
Davis, D.M., Lillie, R.J., 1994. Changing mechanical response during continental collision; active examples from the foreland thrust belts of Pakistan. J. Struct. Geol. 16 (1), 21–34.
Davis, D., Suppe, J., Dahlen, F.A., 1983. Mechanics of fold-and-thrust belts and accretionary wedges. J. Geophys. Res. 88 (B2), 1153–1172.
Dewey, J., Hempton, M., Kidd, W., Saroglu, F., Şengör, A., 1986. Shortening of continental lithosphere: the neotectonics of Eastern Anatolia - a young collision zone. Geol. Soc. Lond. Spec. Publ. 19 (1), 1–36.
Dominguez, S., Lallemand, S., Malavieille, J., von Huene, R., 1998. Upper plate deformation associated with seamount subduction. Tectonophysics 293, 207–224.
Dominguez, S., Malavieille, J., Lallemand, S.E., 2000. Deformation of accretionary wedges in response to seamount subduction: insights from sandbox experiments. Tectonics 19 (1), 182.
Farah, A., Abbas, G., de Jong, K.A., Lawrence, R.D., 1984. Evolution of the lithosphere in Pakistan. Tectonophysics 105 (1–4), 207–227.
Ghiglione, M.C., Cristallini, E.O., 2007. Have the southernmost Andes been curved since Late Cretaceous time? An analog test for the Patagonian Orocline. Geology (Boulder) 35 (1), 13–16.
Gutscher, M.-A., Kukowski, N., Malavieille, J., Lallemand, S.E., 1998. Material transfer in accretionary wedges from analysis of a systematic series of analog experiments. J. Struct. Geol. 20 (4), 407–416.
Hamburger, M.W., Sarewitz, D.R., Pavlis, T.L., Popandopulo, G.A., 1992. Structural and seismic evidence for intracontinental subduction in the Peter the First Range, Central Asia. Geol. Soc. Am. Bull. 104, 397–408.
Hampel, A., Adam, J., Kukowski, N., 2004. Response of the tectonically erosive south Peruvian Forearc to subduction of the Nazca Ridge: analysis of three-dimensional analogue experiments. Tectonics 23 (5), 16.
Haq, S.S., Davis, D.M., 1997. Oblique convergence and the lobate mountain belts of western Pakistan. Geology 25 (1), 23–26.
Hoth, S., Adam, J., Kukowski, N., Oncken, O., 2006. Influence of erosion on the kinematics of bivergent orogens: results from scaled sandbox simulations. Spec. Pap. Geol. Soc. Am. 398, 201–225.
Hoth, S., Hoffmann-Rothe, A., Kukowski, N., 2007. Frontal accretion: an internal clock for bivergent wedge deformation and surface uplift. J. Geophys. Res. 112 (B6), 1–17.
Hsui, A.T., Youngquist, S., 1985. A dynamic model of the curvature of the Mariana Trench. Nature 318, 455–457.
Hubbert, M.K., 1937. Theory of scale models as applied to the study of geologic structures. Bull. Geol. Soc. Am. 48 (10), 1459–1520.
Humayon, M., Lillie, R.J., Lawrence, R.D., 1991. Structural interpretation of the eastern Sulaiman foldbelt and foredeep, Pakistan. Tectonics 10 (2), 299–324.
Keep, M., 2000. Models of lithospheric-scale deformation during plate collision: effects of indentor shape and lithospheric thickness. Tectonophysics 326 (3–4), 203–216.
Keith, C.M., Simpson, D.W., Soboleva, O.V., 1982. Induced seismicity and style of deformation at Nurek Reservoir, Tadjik SSR. J. Geophys. Res. 87 (B6), 4609–4624.
Koons, P.O., 1990. Two-sided orogen: collision and erosion from the sandbox to the Southern Alps, New Zealand. Geology (Boulder) 18 (8), 679–682.
Koulakov, I., Sobolev, S., 2006. A tomographic image of Indian lithosphere break-off beneath the Pamir–Hindukush region. Geophys. J. Int. 164 (2), 425–440.
Lallemand, S.E., Malavieille, J., Calassou, S., 1992. Effects of oceanic ridge subduction on accretionary wedges: experimental modeling and marine observations. Tectonics 11 (6), 1301–1313.
Leith, W., 1982. Rock assemblages in Central Asia and the evolution of the southern Asian margin. Tectonics 1 (3), 303–318.
Leith, W., Alvarez, W., 1985. Structure of the Vakhsh fold-and-thrust belt, Tadjik SSR: geologic mapping on a Landsat image base. Geol. Soc. Am. Bull. 96, 875–885.
Lickorish, W.H., Ford, M., Buergisser, J., Cobbold, P.R., 2002. Arcuate thrust systems in sandbox experiments; a comparison to the external arcs of the Western Alps. Geol. Soc. Am. Bull. 114 (9), 1089–1107.
Linquist, K.G., Engle, K., Stahlke, D., Price, E., 2004. Global topography and bathymetry grid improves research efforts. EOS Trans. Am. Geophys. Union 85 (19), 186.
Lohrmann, J., Kukowski, N., Adam, J., Oncken, O., 2003. The impact of analogue material properties on the geometry, kinematics, and dynamics of convergent sand wedges. J. Struct. Geol. 25 (10), 1691–1711.
Lu, C.-Y., Malavieille, J., 1994. Oblique convergence, indentation and rotation tectonics in the Taiwan Mountain Belt: insights from experimental modelling. Earth Planet. Sci. Lett. 121, 477–494.
Macedo, J., Marshak, S., 1999. Controls on the geometry of fold-thrust belt salients. Geol. Soc. Am. Bull. 111 (12), 1808–1822.
Malavieille, J., 1984. Modelisation experimentale des chevauchements imbriques; application aux chaines de montagnes (Experimental modelling of imbricate overlap; application to mountain ranges). Bull. Soc. Geol. Fr. 26 (1), 129–138.
Marques, F.O., Cobbold, P.R., 2002. Topography as a major factor in the development of arcuate thrust belts: insights from sandbox experiments. Tectonophysics 348 (4), 247–268.
Marques, F.O., Cobbold, P.R., 2006. Effects of topography on the curvature of fold and thrust belts during shortening of a 2-layer model of continental lithosphere. Tectonophysics 415 (1–4), 65–80.
Marshak, S., 2004. Thrust tectonics and hydrocarbon systems: Ch. Salients, Recesses, Arcs, Oroclines, and Syntaxes; a Review of Ideas Concerning the Formation of Map-view Curves in Fold-thrust Belts, Vol. 82, pp. 131–156.
Marshak, S., Wilkerson, M.S., 1992. Effect of overburden thickness on thrust belt geometry and development. Tectonics 11 (3), 560–566.
Masek, J.G., Duncan, C.C., 1998. Minimum-work mountain building. J. Geophys. Res. 103 (B1), 907–917.

Mohadjer, S., Bendick, R., Ischuk, A., Kuzikov, S., Kostuk, A., Saydullaev, U., Lodi, S., Kakar, D.M., Wasy, A., Khan, M.A., Molnar, P., Bilham, R., Zubovich, A.V., 2010. Partitioning of India–Eurasia convergence in the Pamir–Hindu Kush from GPS measurements. Geophys. Res. Lett. 37, 1–6.

Negredo, A.M., Replumaz, A., Villaseñor, A., Guillot, S., 2007. Modeling the evolution of continental subduction processes in the Pamir–Hindu Kush region. Earth Planet. Sci. Lett. 259 (1–2), 212–225.

Persson, K.S., Sokoutis, D., 2002. Analogue models of orogenic wedges controlled by erosion. Tectonophysics 356 (4), 323–336.

Persson, K.S., Garcia-Castellanos, D., Sokoutis, D., 2004. River transport effects on compressional belts: first results from an integrated analogue-numerical model. J. Geophys. Res. 109 (B1), 1–11.

Prasad, A.K., 2000. Stereoscopic particle image velocimetry. Exp. Fluids 29 (2), 103–116.

Ratschbacher, L., Frisch, W., Linzer, H.-G., Merle, O., 1991a. Lateral extrusion in the Eastern Alps, part 2: structural analysis. Tectonics 10 (2), 257–271.

Ratschbacher, L., Merle, O., Davy, P., Cobbold, P., 1991b. Lateral extrusion in the Eastern Alps, part 1: boundary conditions and experiments scaled for gravity. Tectonics 10 (2), 245–256.

Reigber, C., Michel, G., Galas, R., Angermann, D., Klotz, J., Chen, J., Papschev, A., Arslanov, R., Tzurkov, V., Ishanov, M., 2001. New space geodetic constraints on the distribution of deformation in Central Asia. Earth Planet. Sci. Lett. 191 (1–2), 157–165.

Robinson, A.C., Yin, A., Manning, C.E., Harrison, T.M., Zhang, S.-H., Wang, X.-F., 2004. Tectonic evolution of the northeastern Pamir: constraints from the northern portion of the Cenozoic Kongur Shan extensional system, western China. Geol. Soc. Am. Bull. 116 (7–8), 953–973.

Roecker, S.W., Soboleva, O.V., Nersesov, I.L., Lukk, A.A., Hatzfeld, D., Chatelain, J.L., Molnar, P., 1980. Seismicity and fault plane solutions of intermediate depth earthquakes in the Pamir–Hindu Kush region. J. Geophys. Res. 85 (B3), 1358–1364.

Schanz, T., Vermeer, P.A., 1996. Angles of friction and dilatancy of sand. Geotechnique 46 (1), 145–151.

Schellart, W.P., 2000. Shear test results for cohesion and friction coefficients for different granular materials: scaling implications for their usage in analogue modelling. Tectonophysics 324 (1–2), 1–16.

Schreurs, G., Haenni, R., Vock, P., 2001. Four-dimensional analysis of analog models; experiments on transfer zones in fold and thrust belts. Mem. Geol. Soc. Am. 193, 179–190.

Schwab, G., Katzung, G., Ludwig, A.O., Luetzner, H., 1980. Neogene Molassesedimentation in der Tadzikischen Depression (Tadzikische SSR) (Neogene molasse sedimentation in the Tadzhik Depression (Tadjik.SSR)). Z. Angew. Geol. 26 (5), 225–237.

Silver, E.A., Reed, D.L., 1988. Backthrusting in accretionary wedges. J. Geophys. Res. 93 (B4), 3116–3126.

Simpson, G.D., 2010. Formation of accretionary prisms influenced by sediment subduction and supplied by sediments from adjacent continents. Geology 38 (2), 131–134.

Smit, J., Burg, J.-P., Dolati, A., Sokoutis, D., 2010. Effects of mass waste events on thrust wedges: analogue experiments and application to the Makran accretionary wedge. Tectonics 29 (3), 11.

Sobel, E.R., 1999. Basin analysis of the Jurassic–Lower Cretaceous Southwest Tarim Basin, Northwest China. Geol. Soc. Am. Bull. 111 (5), 709–724.

Storti, F., McClay, K., 1995. Influence of syntectonic sedimentation on thrust wedges in analogue models. Geology 23 (11), 999–1002.

Tapponnier, R., Peltzer, G., Le Dain, A.Y., Armijo, R., Cobbold, P., 1982. Propagating extrusion tectonics in Asia: new insights from simple experiments with plasticine. Geology (Boulder) 10 (12), 611–616.

Thomas, J.-C., Chauvin, A., Gapais, D., Bazhenov, M.L., Perroud, H., Cobbold, P.R., Burtman, V.S., 1994a. Paleomagnetic evidence for Cenozoic block rotations in the Tadjik Depression (Central Asia). J. Geophys. Res. 99, 15,141–15,160.

Thomas, J.-C., Gapais, D., Cobbold, P., Meyer, V., Burtman, V., 1994b. Tertiary kinematics of the Tajik depression (Central Asia): inferences from fault and fold patterns: Geodynamic Evolution of Sedimentary Basins, International Symposium, Moscow, pp. 171–180.

Thomas, J.-C., Cobbold, P.R., Wright, A., Gepais, D., 1996. Tectonic evolution of Asia. : Ch. Cenozoic Tectonics of the Tajik Depression, Central Asia. Cambridge Univ. Press, New York, pp. 191–210.

Vlasov, N.G., Dyakov, Y.A., Cherner, E.S. (Eds.), 1991. Geological Map of the Tajik SSR and Adjacent Territories, 1:500,000, Leningrad.

Weijermars, R., Schmeling, H., 1986. Scaling of Newtonian and non-Newtonian fluid dynamics without inertia for quantitative modelling of rock flow due to gravity (including the concept of rheological similarity). Phys. Earth Planet. Inter. 43 (4), 316–330.

Weijermars, R., Jackson, M.P.A., Vendeville, B., 1993. Rheological and tectonic modeling of salt provinces. Tectonophysics 217 (1–2), 143–174.

Wilkerson, M.S., Apotria, T., Farid, T., 2002. Interpreting the geologic map expression of contractional fault-related fold terminations: lateral/oblique ramps versus displacement gradients. J. Struct. Geol. 24 (4), 593–607.

Willett, S., Beaumont, C., Fullsack, P., 1993. Mechanical model for the tectonics of doubly vergent compressional orogens. Geology 21 (4), 371–374.

Zweigel, P., 1998. Arcuate accretionary wedge formation at convex plate margin corners: results of sandbox analogue experiments. J. Struct. Geol. 20 (12), 1597–1609.